Dynamics and thermodynamics of magma mixing: Insights from a simple exploratory model

Frank J. Spera[1], Jason S. Schmidt[2], Wendy A. Bohrson[3,] and Guy A. Brown[4]

[1]Department of Earth Science, University of California, Santa Barbara, CA 93106, USA (corresponding author), spera@geol.ucsb.edu, 805-705-3404 (tele), 805-893-2314 (fax)

[2]Department of Earth Science, University of California, Santa Barbara, CA 93106, USA

[3]Department of Geological Sciences, Central Washington University, Ellensburg, WA 98926

[4]Rocking Hoarse Professional Services, 691 Chelham Way, Santa Barbara, Ca 93108, USA

Abstract

The mixing of magmas of distinct temperature, bulk composition, mineralogy and physical properties plays a central role in explaining the diversity of magma types on Earth and in explaining the growth of continental and oceanic crust. Magma mixing is also of practical importance. For example, the mixing of distinct magmas has been cited as an important process in creation of economically important horizons in layered intrusions as well as a triggering mechanism for initiation of volcanic eruptions. The motivation for better quantifying the dynamics and thermodynamics of magma mixing and its attendant plutonic and volcanic products is clear. The degree of magma mixing, which spans a continuum from mingling to complete hybridization, depends upon initial and boundary conditions, magma properties, driving forces and time available for mixing. Magma mingling produces a heterogeneous mixture of discrete clumps of the end-member magmas, whereas complete hybridization involves the thermodynamic equilibration of two distinct magmas to form a third. Qualitatively, mixing occurs *via* reduction in the size of compositional heterogeneities (i.e., clumps) through stretching and folding by viscous flow, followed by homogenization, once shear has reduced the size of compositional anomalies to diffusive length scales. Quantification of this process relies on two statistical measures: the linear scale of segregation (Λ) defined as the spatial integral of the compositional correlation function related to the size-distribution of the segregated clumps within the mixture, and the intensity of segregation (I) a measure that quantifies how much the composition at each location differs from the average. The mixing dynamics of a layered system are analyzed in terms of the parameters governing mixing (Rayleigh, Lewis and Buoyancy numbers and viscosity ratio) to estimate how the timescale for magma hybridization, τ_{H}, compares to solidification, recharge, diffusive and assimilation timescales. This analysis illustrates that hybridization times can be shorter than or comparable to thermal, solidification and replenishment timescales; thus, formation of hybridized or nearly hybridized magmas is one anticipated outcome of mixing. The machinery of thermodynamics can be used to compute the hybrid magma state. An exploratory model for the thermochemistry of hybridization is developed based on binary eutectic phase relations and thermodynamics. Eight thermodynamic parameters define the phase diagram and associated energetics, and six parameters (initial temperatures, compositions, mass ratio of mixing magmas and an enthalpy parameter) are necessary and sufficient to determine the state of hybrid magma uniquely. While relevant combinations of 14 thermodynamic and mixing parameters might suggest that the number of mixing outcomes (i.e., products) is too high to systematize, Monte Carlo simulations using the exploratory model document how millions of arbitrary initial states evolve into five possible final (mixed) states. Such an analysis implies that a magma mixing taxonomy that defines possible mixed product states can be developed and tied to petrologic indicators of mixing. Additional insights gained from this exploratory model that are supported by independent results from a multicomponent, multiphase thermodynamic model of magma mixing (Magma Chamber Simulator) include: (1) the proclivity of invariant point hybrid states, which may explain some instances of compositionally monotonous melts associated with mixed magma eruptions; (2) a surprising thermal effect such that the temperature of hybridized magma can be

137 significantly *less* than the initial temperature of *either* of the mixing magmas. This type
138 of magma mixing may result in crystal resorption, thus invalidating an assumption that
139 resorption textures in crystals are typically the result of a magma heating event; (3)
140 illustration of the differing effects of stoped block temperature and composition on hybrid
141 magma temperature and phase state, and (4) illustration of a cessation of crystallization
142 effect that may pertain to the MORB pyroxene 'paradox'. Differences between adiabatic
143 or R-hybridization and diabatic or RFC-hybridization are also explored. The model can
144 be used to elucidate the thermodynamic principles underlying magma mixing in the
145 hybridization limit. These principles are of general applicability and carry over to more
146 compositionally complicated systems.
147
148

Introduction

The proposition that the mixing of magmas of distinct temperature, bulk composition, and phase state (i.e., phase composition and abundance) is an important petrogenetic process is almost as old as the discipline of igneous petrology (Bunsen, 1851; see Wilcox, 1999 for historical review). Abundant evidence in support of magma mixing (mafic magma addition to resident silicic magma or *vice versa*) is derived from studies of mafic enclaves in plutonic rocks (e.g., Pabst, 1928; Didier and Barbarin, 1991), syn-plutonic mafic or silicic dikes within intrusive bodies (e.g., Blake et al., 1965; Wiebe, 1973; Reid et al., 1983; Furman and Spera, 1985; Wiebe, 1987, 1996; Baxter and Feely, 2002; Gibson et al., 2003; Wiebe and Hawkins, in Press) and from abrupt changes in cumulate rock modes and phase compositions in layered intrusions (e.g., Wager and Brown, 1968; Irvine, 1970; McCallum et al., 1980; DePaolo, 1985; Eales, 2002; Morse, 2008; Vantongeren and Mathez, 2013). Additionally, mixed-pumice eruptions (e.g., Anderson, 1976; Smith, 1979; Eichelberger, 1980; Bacon, 1986; Nakamura, 1995; Coombs et al., 2000; Eichelberger et al., 2013) and crystal-scale heterogeneity in phenocrysts and cumulate minerals (e.g., Dungan, 1987; Stelten et al., 2013; Humphreys et al., 2013) provide *prima facie* evidence for the mixing of magmas. Magma recharge and mixing are key elements of modern theories of petrogenesis, and the significant contribution magma mixing makes to petrogenesis in a range of petrotectonic environments including MORB (Walker et al., 1979), Island Arcs (Sakuyama, 1984) and Ocean Island Basalts (OIB) (Kamber and Collerson, 2004) cannot be overemphasized. The key point is that magmas evolve in open systems exchanging heat and material with their surroundings. Magma recharge is an important agent of this dynamical behavior.

The dynamics of viscous fluid (*sensu lato*) mixing is a complex subject with an extensive literature (e.g., see reviews in Ottino, 1989; Haller, 2001; Voth et al., 2002). Mixing is widespread in nature and in myriad technological applications. In the geosciences, mixing is relevant to the oceans (Poje and Haller, 1999), atmosphere (Koh and Legras, 2002), mantle (Farnetani and Samuel, 2003; Tackley, 2007; Le Bars and Davaille, 2004) and at smaller scales in continental hydrological, hydrothermal, and magmatic systems. In this work, attention is focused upon the dynamics and thermodynamics of magma mixing. In particular, the dynamics of magma mingling and

mixing is examined for a canonical layered magma body in order to provide estimates of the magma hybridization time. This is the time required for two initially distinct magmas to intimately hybridize and achieve thermodynamic equilibrium.

When two magmas are stirred together, a wide range of outcomes is possible. A particular outcome depends upon the imposed initial and boundary conditions, the initial spatial configuration of the magmas, magma thermodynamic and transport properties, the relative forces that drive mixing, and the time available for mixing before arrest by freezing (plutonic) or quenching (eruption). In broad terms, the phenomenon of mixing is simply viewed as the progressive (temporal) eradication of compositional heterogeneities (i.e., clumps) by stretching and folding due to the action of viscous shearing forces. Pressure, buoyancy, and inertial forces potentially contribute to these motions. Once shear mixing has reduced the size of chemical anomalies to diffusive length scales, homogenization is achieved by chemical diffusion (Ottino, 1989).

Historically, when magma mixing has been invoked as a petrogenetic hypothesis the terms 'mingling' and 'hybridization' have been used differently by different geologists. In order to be precise, the following conventions are used in this work. Magma mixing occurs along the spectrum from mingling to hybridization. *Mingling* of magmas produces a heterogeneous mixture containing discrete portions (clumps) of the end-member magmas (hereafter called **M** for resident magma and **R** for recharge magma). The final product comprises spatially discrete portions of each magma type distributed heterogeneously within the magma body. Hybridization involves the mixing and thermodynamic equilibration of two or more distinct magmas to form a chemically and physically homogeneous magma (hereafter called **H** for hybrid magma). Magma hybridization can be studied as an adiabatic (isenthalpic) or diathermal (diabatic) process. It is noted that whereas the dynamics of magma mixing is indeed a very complicated fluid dynamical problem, in the hybridization limit, the machinery of equilibrium thermodynamics allows determination of the state of hybridized magma provided appropriate and sufficient thermodynamic data are available without recourse to dynamics *per se*. It is important to note that 'perfect' hybridization (as defined here) generates a homogeneous magma that preserves no record of the mixing process itself. It represents a thermodynamic equilibrium limit. In practice, one may anticipate that there

exists a 'scale of scrutiny' below which heterogeneity reigns. In a later section, a statistical quantity, the linear scale of segregation (Λ), is introduced to quantify the extent of heterogeneity. This statistical measure of dimension length allows one to gauge the spatial scale at which the magma body is indeed mixed. Finally, it is noted that although, as defined in this study, a hybrid (homogeneous) magma results from the complete mixing of two (or more) end-member magmas, not every homogeneous magma is the result of hybridization. For example, partial melting of a source at or near an invariant point can generate a homogeneous magma that has nothing to do with magma mixing.

The purpose of this study is two-fold. In the first part, a brief treatment of magma mixing dynamics is presented to illustrate how the extent of mixing can be quantified using simple statistical measures. Estimates for magma hybridization times as a function of the critical parameters for an initially compositionally layered system are presented. Analysis shows that hybridization times can be shorter than or comparable to thermal, solidification and replenishment timescales (Oldenburg et al., 1989; Petrelli et al., 2011), a feature that facilitates the formation of hybridized magma following mixing of two distinct magmas. The second goal is to develop and apply a simple exploratory model of the thermochemistry of magma hybridization for both adiabatic and diabatic mixing. The model is based on a binary system (e.g., $CaMgSi_2O_6$-$CaAl_2Si_2O_8$) with simple thermodynamics (ideal mixing, eutectic phase equilibria, no crystalline solution). The function of this exploratory or 'toy' model is to elucidate the principles of magma hybridization without any obfuscating details (e.g., Larson et al., 2014). The 'toy' model of Dyson (2000) pertaining to the origin of life is a classic example illustrating the power and role toy models play in the elucidation of the fundamental aspects of a complex natural system, whether biological or physiochemical. For magma mixing, the effects of arbitrary variations in bulk composition, temperature, and mixing ratio (**M** to **R**) on hybridization outcomes are explored in temperature-enthalpy-composition coordinates. Behaviors observed in the exploratory model also appear in more complete multicomponent-multiphase calculations using the Magma Chamber Simulator (MCS, Bohrson et al., 2014) and highlight the resulting challenges to identify associated characteristics in natural mixed systems. A key conclusion from numerous simulations

using the exploratory and MCS models is that magma (multiphase) mixing is very different than the mixing of two melts to form a third homogeneous melt. When two melts blend to form a third melt, the final temperature of the hybridized melt is the mass-weighted average of the temperatures of the mixing liquids (unless the heat of mixing is very different than zero, which is rarely the case in silicate liquid mixing), and the final melt composition is the weighted average of the compositions of **M** and **R** melts. But the mixing of aphyric melts is uncommon because superheated magmas are rare in Nature (Carmichael et al., 1974). These melt-melt mixing relations are not followed when two magmas mix, and thus intuition about mixing developed using melt-melt mixing relations may lead to erroneous conclusions about the mixing process and products. As we demonstrate, the temperature of the hybrid magma can be below that of **M** and **R,** and the melt composition can be markedly different than the bulk composition of the hybrid magma. Exploration of the possible outcomes of magma hybridization using the toy model therefore provides insight into the thermochemistry of magma mixing in Nature and permits identification of characteristics of mixed systems that may have gone previously unrecognized. An excellent guide to the application of magma mixing thermodynamics to MORB magmas is given in Walker et al (1979).

Quantification of Magma Mixing: Mingling versus Hybridization

Magma Mixing Definition and Terminology

Magma mixing is the process of bringing two initially distinct magmas together and allowing an approach to equilibrium to be made. In magma mingling two initially distinct magmas, **M** and **R**, remain compositionally distinct (e.g., as discrete co-mingled volumes of one within the other) except for very thin (mm-cm) interfacial diffusive boundaries. In magma hybridization, **M** and **R** thoroughly mix and thermodynamic equilibrium is achieved. The resultant hybrid magma (**H**) is a mixture of homogeneous melt, unzoned crystals, and bubbles of supercritical fluid (when fluid saturated). In **H** magma, all coexisting phases are at a unique and identical temperature and pressure, and the chemical potentials of all components in all phases are equal. Hybridization is thus a unique end-member state of the phenomenon of magma mixing. When hybridization

occurs at constant enthalpy (isenthalpic), no heat is removed from the system and hence the enthalpy of the hybrid magma (**H**) is identical to the sum of the (appropriately mass-weighted) enthalpies of **M** and **R** magmas (the mixing 'components'). This process is defined as Recharge-hybridization or R-hybridization. Alternatively, when mixing is accomplished under diathermal conditions (i.e., diabatic mixing), the ratio of the enthalpy of **H** magma (h^H) to the sum of the mass-weighted enthalpies of **M** and **R** (h^M and h^R, respectively) is Φ ($0<\Phi<1$). Diathermal mixing is termed RFC- hybridization since the hybridized magma reflects concurrent recharge, performed isenthalpically, and crystallization, a diabatic process driven by heat removal. Crystallization can be either fractional or equilibrium. In natural systems, crystallization is usually closer to fractional than equilibrium, although 'perfect' fractional crystallization is rarely attained. Incremental batch crystallization is probably a better model, in general (Langmuir, 1989; Bohrson et al., 2014). Although not pursued in this study, partial melting can also be studied using the toy model by allowing $\Phi>1$. In this case, the ratio of the enthalpy of the hybrid magma to the enthalpy of the mass-weighted average of distinct crystalline sources (**M** and **R**) equals Φ with Φ>1. Physically, this corresponds to partial melting driven by addition of heat to a crystalline source.

Quantitative Measures of Magma Mixing

It is important to establish quantitative measures of the 'goodness of mixing'. Indeed, many methods have been developed to analyze the time-dependence of mixing dynamics. These include, for example, mapping of Poincare sections, the determination of finite-size and finite-time Lyapunov exponents from concentration variations in space and time, and calculation of hyperbolic persistence times. Mixing time estimates extracted from these measures involve knowledge of velocity, temperature and compositional fields for particular flow configurations with well-defined boundary and initial conditions and rely on sophisticated mathematical manipulations of these data (e.g., Liu et al., 1994; Farnetani and Samuel, 2003; van Keken et al., 2003; Tackley, 2007). These methods are difficult if not impossible to apply to 'snapshots' of magmatic systems observed in the field when studying volcanic and plutonic rocks, however. To overcome this problem, two statistical parameters, developed by Danckwerts (1953a, 1953b) for

chemical reactor analysis and applied by Oldenburg et al (1989) and Tedesco and Spera (1992) to magma mixing, are considered here. These statistical measures are the linear scale of segregation Λ and the intensity of segregation I. The advantage of these metrics is that they can be applied independent of knowledge of the temporal evolution of the mixing process because they solely utilize information on the observed spatial pattern of heterogeneity. That is, they can be applied to a 'snapshot' of a compositional field.

Magma mingling is characterized by a reduction in size of compositional anomalies (deviations from the mean composition), and the linear scale of segregation (Λ) is useful in quantifying the mixing state of the system in terms of its 'clumpiness'. The linear scale of segregation is based upon deviations from the mean defined by $C_1 - \bar{C}$ and $C_2 - \bar{C}$ where C is shorthand for an array of compositional variables such as the mass fraction of oxide components or the concentration of a trace element and the subscripts refer to distinct locations in Euclidean space within the mixing domain separated by distance r. In well-mixed (homogenous) magma, such deviations are identically zero everywhere. The average of the product of these deviations over many distinct pairs all distance r apart is denoted $\overline{(C_1 - \bar{C})(C_2 - \bar{C})}$. If this summation is repeated over all possible pair separation distances (i.e., different values of r, the separation distance) and the resulting quantity is divided by the mean square compositional deviation (the variance) $\overline{(C - \bar{C})^2}$, then a normalized correlation function

$$R(r) = \frac{\overline{(C_1 - \bar{C})(C_2 - \bar{C})}}{\overline{(C - \bar{C})^2}} \qquad (1)$$

is formed. It is noted that when r = zero, $C_1 = C_2$, and R(0) = 1; that is, at separation distance zero, the mixture is completely segregated. In general, values of R(r) near 1 mean that a concentration greater or less than the mean at some point in the magma is likely to be correlated with a similar positive or negative compositional anomaly a distance r away. If R(r) = 0, a random relationship exists between concentrations at the two locations separated by distance r. A value of R(r) near -1 means that there is a perfect anti-correlation between the magma compositions at the two locations, for instance, if pure 'silicic' melt is at one location, and pure 'basalt' is at the other. The linear scale of segregation Λ is defined as the integral of the normalized correlation function

333

$$\Lambda = \int_0^{r_{max}} \mathrm{R(r)dr} \qquad (2)$$

334

335 Because Λ is evaluated over a large range of r, it is a measure of the 'lumpiness' of the
336 compositional anomalies at spatial scales greater than typical diffusive scales that are of
337 order mm to cm in magmas.

338 A second metric, the intensity of segregation I, is a scalar measure of magma
339 homogeneity relating the compositional anomaly at a given location relative to the mean
340 composition ($\bar{C}$) over the volume of the body. The intensity of segregation (I) is defined

341 $$I = \frac{\overline{(C-\bar{C})^2}}{\bar{C}(1-\bar{C})} \qquad (3)$$

342 where the numerator is the variance of the compositional field. The intensity of
343 segregation is essentially a rescaled variance. It measures how much the composition at
344 each point differs from the average composition of the mixture. I has the value of 1 when
345 segregation is complete (e.g., the concentration at every point is either 'silicic' or
346 'basaltic'), and I = 0 when the composition is uniform and the mixing end-members have
347 been hybridized to form a homogeneous magma. I reflects neither the relative amounts of
348 the two initially distinct magmas nor the size of the clumps. Instead, I measures the
349 extent to which the initially distinct magmas vary in composition from the spatial average
350 throughout the mixing domain. A perfectly clumpy two 'component' mixture with no
351 intermediate composition has an Intensity (I) of unity no matter what the size of the
352 clumps may be.

353 Qualitatively, the linear scale of segregation (Λ) can be pictured as the size of the
354 segregated clumps within the mixture, while the intensity of segregation (I) describes the
355 difference in composition between a clump and surrounding magma. Small scale mixing
356 in magmas proceeds by decreasing both the scale and intensity of segregation. The
357 intensity of mixing is a monotonically decreasing function of time due to diffusion, in
358 accordance with the Second Law of Thermodynamics. The scale of segregation, although
359 eventually decreasing to zero when hybridization is complete, does not necessarily do so

monotonically (Oldenburg et al., 1989 and see below). It is recognized that any magmatic mixture, if examined closely enough, will show regions where the composition varies from point to point. The maximum size of a segregated region varies depending upon the level of scrutiny commensurate with the objectives of the petrologic study.

Based on the indices of the 'goodness of mixing' defined above, some limiting cases can be described. At the initiation of mixing, I is equal to unity and Λ is equal to some maximal linear scale depending on the pre-mixing configuration. For example, for the canonical 'before mixing' configuration of a layered magma body such as silicic 'cold' magma of thickness λ_S atop an equal thickness of mafic 'hot' magma, the linear scale of segregation at t = 0 is simply λ_S. In any mixing process with nonzero diffusion, $I \to 0$ as $t \to \infty$ because once normal and shear strain reduces compositional anomalies to diffusive lengths, the anomalies are erased by molecular diffusion. Similarly, as $t \to \infty$, $\Lambda \to 0$ since the linear scale of segregation evolves to zero after a sufficiently long duration of stirring when clumps are vanishingly small. Of course the crux of the issue in magma mixing is to quantify precisely the duration of a 'sufficiently long' time interval. To make estimates of the mixing time in general is not easy; a plethora of details regarding the flow dynamics and configuration and properties of the mixing magmas must be defined quantitatively. Fortunately, for the canonical arrangement of a layered magma system, enough is known presently to make rough estimates of mixing times. In the following section this problem is considered in more detail.

Magma Mixing Dynamics

Although incomplete magma mixing, evidenced by petrographic and field-scale disequilibrium features, is ubiquitous, examples of magmas hypothesized to originate *via* hybridization, of two initially distinct end-member magmas are not uncommon (e.g., Dunham and Wadsworth, 1978; Hibbard, 1981, 1991; Browning, 1984; Dungan, 1987; Gibson et al., 2003; Appleby et al., 2008). Accordingly, before discussing the thermodynamics of hybridization, a discussion of the dynamics of mixing with emphasis on the factors that control the time required for two magmas to mix sufficiently thoroughly to approximate the hybridized state ($I \approx 0$ and $\Lambda \approx 0$) is presented. The main

conclusion is that hybridization timescales are of the same order or less than timescales associated with magma cooling, crystallization and magma chamber growth itself. It is therefore reasonable to expect to encounter examples where magma hybridization has gone to completion or nearly to completion in natural systems. Indeed, as noted above, many such examples can be found by examination of the petrological literature. It is emphasized that the 'level of scrutiny' is an important aspect in recognizing the attainment of hybridization. In the strict sense, a hybridized magma has $I = \Lambda = 0$, exactly. In practice, the level of scrutiny, defined as a length scale, comes into play in the determination of whether magma mixing has created a hybrid magma. If zonation in phenocrysts can be 'tolerated', then $\Lambda \approx 1\text{mm}$. If the level of scrutiny is zoning at the small crystallite scale, $\Lambda \approx 10\,\text{microns}$. On the other hand if the scale of scrutiny is no smaller than typical glomeroporphyritic clots, then hybridization has been achieved to the limit of $\Lambda \approx 10^{-2}\,\text{m}$.

The magma hybridization timescale (τ_H) is the time interval following the onset of magma mixing required for the distinct magmas to achieve thermodynamic equilibrium *via* the mixing process. Quantitatively, this implies a hybrid (**H**) magma with mixing statistics of $I \to 0$ and $\Lambda \to 0$ where the practical limit is based on an appropriate 'scale of scrutiny' based on the type of petrologic study and geochemical tools used to characterize the state of the system (e.g., field, petrographic, microprobe, laser ablation of single phenocrysts, etc.). Once defined, τ_H can be compared with solidification, recharge, diffusive and assimilation timescales in order to recognize the chronological dynamics of petrogenesis (e.g., see discussion in Bohrson et al., 2014 for these scales). When the hybridization timescale is less than other transport timescales, magma mixing can approach 'completion' and hybrid magma is formed. Unfortunately, there is no comprehensive picture of possible mixing outcomes for arbitrary mixing scenarios. In this study, attention is focused on the dynamics of mixing for the simple case of an initially layered magma body. This is an archetypical configuration; many previous numerical, laboratory and field studies (e.g., Sparks et al., 1977; Huppert et al, 1982; Olson et al., 1984; Clark et al, 1987; Oldenburg et al, 1989; Todesco and Spera, 1992; Wiebe, 1996; Jellinek and Kerr, 1999; Davaille, 1999a,b; Le Bars and Davaille, 2002, 2004a, 2004b, Petrelli et al., 2006, 2011) have focused on this configuration in an effort

421 to approximately estimate the dependence of hybridization time on magma properties and
422 volumes.

423 The geometry, magma properties, and boundary conditions of the mixing
424 configuration are depicted in Figure 1. In Table 1, all parameters are defined. For
425 simplicity, it is assumed that the starting **M** and **R** compositions are one-phase liquids to
426 avoid phase equilibria considerations. The melt density is a function of temperature (T)
427 and composition, where C is the mass fraction of light component, and **M** and **R** refer to
428 the distinct magmas that are mixed and subsequently hybridized. Following Clark et al.
429 (1987), the equation of state is

430 $$\rho(T,C) = \rho_{T_o^R, C_o^R}\left[1 - \alpha_T(T - T_o^R) - \alpha_C(C - C_o^R\right] \qquad (4)$$

431 where the reference density, $\rho_{T_o^R, C_o^R}$, is the melt density at the initial temperature and
432 composition of the bottom (**R)** layer where $T = T_o^R = T_b$ and $C = C_o^R$, α_T and α_C are the
433 melt thermal and chemical expansivities, respectively, and ρ is melt density. It is
434 convenient to use dimensionless variables for temperature and composition. These are
435 defined $\hat{T} = (T - T_o^M)/(T_o^R - T_o^M)$ and $\hat{C} = (C - C_o^R)/(C_o^M - C_o^R)$. In the initial state, the
436 difference in density between **R** (bottom layer) and **M** (top layer) is
437 $\Delta\rho = \rho_{T_o^R, C_o^R}\left(\alpha_C \Delta C - \alpha_T \Delta T\right)$ where $\Delta T = T_{bottom} - T_{top}$, $\Delta C = C_o^M - C_o^R$ and the reference
438 density is the density of melt at $T = T_o^R = T_b$ and $C = C_o^R$. For example, if dacitic melt sits
439 atop andesitic melt and composition is parameterized on mass fraction silica, typical
440 parameters are T_o^R = 1373 K, $T_o^M = T_t$ = 1173 K, α_C = 0.8, $\alpha_T = 4 \times 10^{-5}$ K^{-1}, C^M = 0.7, C^R
441 = 0.6 and hence $\Delta\rho \approx 200$ kg/m^3 for a reference density of 2700 kg/m^3 (i.e., **R** magma is
442 200 kg/m^3 denser than **M** magma in the initial state). Values of α_C for various oxide
443 components may be found in Clark et al. (1987). Values of $\alpha_C \Delta C$ depend on the
444 particular oxide component and the compositional differences between the layers. For the
445 extreme case of a basalt-rhyolite layered arrangement, the magnitude of the product
446 $\alpha_C \Delta C$ varies from ~0.01 to 0.3 for the major oxide components. The two largest values
447 are for silica (0.13) and H_2O (0.3); thus, the importance of having quantitative constraints
448 on the H_2O content of the end-member mixing magmas is obvious. A typical value for

449 $\alpha_T \Delta T$ is ~ 0.01. This shows that, in general, buoyancy effects due to differences in
450 composition outweigh those due to temperature. The dynamical significance of this is
451 discussed below.
452 The dimensionless parameters that govern the stability and evolution of the
453 layered arrangement of Figure 1 include the thermal Rayleigh number, $\mathrm{Ra}=\frac{\alpha_T g \Delta T d^3}{\nu_R \kappa}$,
454 the buoyancy number (the ratio of chemical to thermal buoyancy), $B=\frac{\alpha_C \Delta C}{\alpha_T \Delta T}$, the Lewis
455 number, $\mathrm{Le}=\frac{\kappa}{D}$ (where κ is the thermal diffusivity and D is the diffusivity of chemical
456 species), the kinematic viscosity ratio $\nu_r=\frac{\nu_M}{\nu_R}$, and the thicknesses of the two layers.
457 (See Table 1 for definitions of equation parameters not given here). The kinematic
458 viscosity ratio depends on T and C, although typically the C-dependence is more
459 important (Spera, 2003). In what follows, the layers are of identical thickness for
460 simplicity. In magma systems, Ra varies widely, from 10^8-10^{16} or larger due mainly to
461 the range in magma body size ($d \sim V^{1/3}$; V is magma body volume) and to a lesser extent
462 on magma kinematic viscosity. Le is typically large, of order 10^5 for most chemical
463 species. Range for the buoyancy number B is discussed below.
464 The effects of Ra, Le and B have been studied by laboratory and numerical
465 methods for the layered arrangement of Figure 1 for a limited range of the governing
466 parameters; these results can be applied to magma mixing scenarios, approximately. A
467 useful way to discuss magma mixing scenarios is to hold Ra and Le fixed and study the
468 effects of the buoyancy number B on flow dynamics, entrainment rates, and hybridization
469 times. The discussion that follows assumes $\mathrm{Ra} \sim 10^8$ and $\mathrm{Le} \sim 10^5$ as a starting point
470 because these values have been studied experimentally and because simulations at much
471 higher Rayleigh numbers are not practical due to computational resource limitations.
472 Although this may appear as a severe limitation, scaling studies show that hybridization
473 times scale as $\tau_H \sim \mathrm{Ra}^{-1} B^2 \mathrm{Le}^{1/2} \nu_r^{1/2}$ (Oldenburg et al., 1989; Petrelli et al., 2011). Hence,
474 the effects of more realistic Ra values can be approximated using this scaling relationship.
475 Note that the hybridization timescale depends most strongly on buoyancy number B.

In general B can be positive, zero or negative. For B >1, compositional buoyancy is strong and a stable stratification develops (e.g., 'rhyolite over basalt'). Although each layer may experience internal convective overturn due to the temperature gradient, the interface between the two compositions remains flat and entrainment rates and mass exchange between layers is small. For B>>1, mass exchange is governed solely by diffusion with very limited entrainment (mass exchange) between the layers. The interfacial diffusive layer thickness scales as $\delta = \sqrt{Dt}$ where t is the duration of contact. Based on a tracer diffusivity of oxygen in a silicate melt of 10^{-12} m^2/s at 1500 K (Lesher and Spera, 2015), diffusive boundary layer thicknesses are 0.8 mm, 1.6 mm, 5.6 mm, 1.8 cm, 5.6 cm, and 0.18 m for durations of a week, month, year, decade, century, and millennium, respectively. These chemical boundary layers are much thinner than characteristic lengths of magma bodies, consistent with minimal mass exchange. Because conductive transfer of heat is faster than species diffusion by ~ 10^5 or more, heating of the overlying silicic magma advances more quickly. For example, heat travels 0.5 m, 1 m, 3.5 m, 11 m and 110 m for durations of a week, month, year, decade, century, and millennium, respectively. Thus, for B>>1, the lower part of the top layer will acquire positive thermal buoyancy if heated from below. When the thickness of the basal thermal layer h_c exceeds a critical value, the layer will be unstable (unless stabilized by internal layer compositional buoyancy), detach and flow upwards as a buoyant plume. The thickness of the basal layer is approximately $h_c = \left(\kappa \eta^M Ra_{crit} / \rho_o \alpha^M \Delta T g\right)^{1/3}$. For typical values appropriate for an andesitic bulk composition and $Ra_{crit}= 10^3$, the critical thickness is several meters (Spera, 2003). This layer can develop within weeks after **R** and **M** are juxtaposed. The stirring and decompression associated with ascent of the thermally buoyant layer (plume) could in turn trigger an instability driven by volatile exsolution *via* Rayleigh-Taylor instability. For example, if basal layer **M** magma happens to be close to volatile saturation, then ascent and decompression could drive the magma locally to volatile saturation and potentially trigger dynamical behavior leading to an eruption. This is the eruption 'trigger' mechanism of Sparks et al. (1977) and is contingent on the details of the H_2O content of **M,** local temperature and the vigor of plume ascent. The ascent velocity, when a plume detaches can be roughly estimated for this Rayleigh-Taylor

instability by balancing viscosity against thermal buoyancy according to $v \approx \frac{g\rho_o \alpha \Delta T h_c^2}{\eta}$. Typical values appropriate for dacitic magma gives ~ 0.01m/s, which is quite rapid.

For $0.5 < B < 1$, dynamic topography develops along the interface with an amplitude that grows as $Ra^{1/3}$, approximately (Gurnis and Davies, 1986). This leads to moderate entrainment and the decrease in both the linear scale of segregation and intensity of segregation with time. For B values, $0.3 < B < 0.5$, doming flow modes occur with extreme tilting of the interface (e.g., see Todesco and Spera, 1993; Le Bars and Davaille, 2004 for examples from computation and laboratory experiments, respectively). In these flows, the linear scale of segregation decreases temporally (although not monotonically) as the interface between **M** and **R** sloshes to and fro. Domes of **R** within **M** oscillate with a period that depends on Ra. The rate of change of segregation intensity I is inversely proportional to B and increases for increasing Ra. At the lower end of the B range, dome heights approach layer thicknesses and rapid overturn, entrainment, and mixing can occur by 'breaking wave' dynamics (e.g., Todesco and Spera, 1993). In this case, small clumps (~0.1 m) of unmixed **M** and **R** magmas remain compositionally intact and crystals, some from **M** and some from **R,** would be mixed, partially re-equilibrated and might exhibit complex disequilibrium features, especially when the viscosity ratio of the mixing magmas is large and for crystals with small intracrystalline diffusion rates like albite-anorthite zoning in plagioclase. Relatively unzoned crystals in local equilibrium with hybrid melt might also be present in regions where Λ has produced small clumps of diffusive length scale (mm) that can be eradicated in periods of order years to decade. This sort of complex textural and compositional evidence is ubiquitous in the geologic record (e.g., Clynne, 1999, Landi et al. 2004; Salisbury et al., 2008; Tepley et al., 2000; Troll and Schmincke, 2002). The timescale for this mixing is 0.3-0.5 of the thermal timescale $\tau_T = d^2/\kappa$. For example, with d~1 km, the thermal timescale is $\tau_T \approx 33\,\text{ka}$ and the hybridization timescale τ_H is about 13 ka.

Finally, for $0 < B < 0.2$, rapid overturning occurs and mixing proceeds very rapidly in a small fraction (~0.05) of the thermal diffusion time. For scale, a 1 km thick **M+R** layered system has a thermal timescale of ~33 ka. Hence for small positive B,

mixing is efficient within decades to centuries to a millennium depending most significantly on the volume of the system and magma physical properties.

For B = 0, mixing of **M** and **R** liquids is driven solely by thermal convection. This is the special case of 'passive' scalar or tracer mixing, for which there is no compositional buoyancy. That is, the chemical anomaly generates no intrinsic density difference and hence there is no buoyancy force due to composition. The mixing of two magmas of essentially identical major element bulk composition but different trace element concentrations would be an example of passive mixing (e.g., **R** magma is doped with a passive tracer, such as a trace element, with negligible effect on melt density). The hybridization time (τ_H) for the mixing of a passive tracer can be estimated from models and numerical experiments (e.g., Kellogg and Turcotte, 1990; Coltice and Schmalzl, 2006) using scaling relations for high Rayleigh number convection for velocity and boundary layer thicknesses from Spera (1992). Mixing occurs by Lagrangian stretching of clumps to sizes that are then erased by diffusion. Melt clumps may be of different viscosity. The hybridization time (τ_H) depends weakly on the tracer diffusivity and is most sensitive to Ra and the thickness of the combined layers, d. For **M** and **R** of equal volumes and densities, the time for homogenization is

$$\tau_H \approx \frac{d^2 \nu_r^{2/3}}{2\kappa a} Ra^{-b} \ln\left(\frac{a\kappa \nu_r^{2/3} Ra^b}{D}\right) \qquad (5)$$

where a = 0.023 and b = 0.685 are constants relating the Lagrangian bulk strain rate to the Rayleigh number. For typical parameters related to mixing of mafic and intermediate composition melts with a viscosity contrast of 100 (d = 1 km, ν_r = 100, $\kappa = 5 \times 10^{-7}$ m^2/s, $\alpha = 2 \times 10^{-5}$, D = 10^{-12} m^2/s), the mixing time is roughly 8 months, a tiny fraction of the thermal lifetime of the system. Note that the hybridization time scales as the 2/3 power of the viscosity ratio. So, for example, if the layers are of equal viscosity, the hybridization time is reduced to $\tau_H \sim$ four days. For an extreme case of viscosity contrast with viscous melt (~10^7 Pa s) above less viscous melt (100 Pa s), the hybridization time is 100 times longer or about 70 years. Of course, in the latter case, if a significant density difference exists between the magmas, dynamically passive mixing is not appropriate and mixing

565 times would be longer. The timescale for hybridization is proportional to B^{-1} or B^{-2}
566 depending on prevailing conditions (e.g., Oldenburg et al., 1989; Davaille, 1999a, 1999b;
567 Gonnermann et al., 2002).

568 In conclusion, the mixing times estimated here are consistent with field
569 observations of mixed magmas in volcanic and plutonic environments spanning the range
570 from little to no mixing through various stages of magma mingling observed as
571 incomplete mixing and finally to essentially complete homogenization or magma
572 hybridization at some appropriate scale of scrutiny of order mm to cm. In the latter case,
573 attainment of thermodynamic equilibration has essentially been reached and the resulting
574 homogeneous magma is identified as hybrid (**H**) magma. Making the connection between
575 laboratory and numerical studies of magma mixing with quantified examples from the
576 geologic record, using the statistical tools of the scale and intensity of segregation is an
577 important future goal. Attention has focused here on the archetypical case of a layered
578 magma system although nature is certainly more complicated. Regardless of the
579 complexities of the fluid mechanics of magma mixing, in the end-member case of magma
580 hybridization, the state of the hybridized magma can be determined by thermodynamics
581 since the linear scale of segregation and intensity of segregation are small numbers,
582 approaching zero. The thermodynamics of hybridization, valid in the limit $\Lambda = \mathrm{I} \to 0$, is
583 illustrated using an exploratory model in the remainder of this study.
584

585 ## Magma Hybridization: Formulation of an Exploratory Model

586 ### Introduction

587 Magma hybridization represents the end-member limit of magma mixing when
588 thermodynamic equilibrium is attained. Transport phenomena are not relevant in this
589 limit; it is assumed that adequate time has passed to attain a well-mixed equilibrium state.
590 As noted above, the temporal chemical evolution of magma mixing is rather complicated,
591 even in idealized scenarios such as 'dense/hot' below 'light/cool'. Although magma
592 hybridization is an end-member process, much can be learned by study of the
593 thermochemistry of hybridization. In order to better understand the relationship between
594 the state and properties of the mixing magmas (**M** and **R**) and resultant hybrid (**H**), an
595 exploratory or 'toy' model for magma hybridization based on isobaric binary eutectic

phase relations has been developed. This model is used to study the taxonomy of magma hybridization; specifically, how various initial states evolve into one of a few possible final states. In addition, a surprising thermal effect in which the temperature of hybridized magma can be significantly less than *either* of the mixing magmas is presented and discussed. Calculations based on the Magma Chamber Simulator (Bohrson et al., 2014) are used to verify that this unexpected thermal effect in fact occurs in multicomponent-multiphase systems and is not an artifact of the simplicity of the toy model. Examples of the effects of stoped wholly crystalline blocks and reaction of mushy blocks with resident magma are also given. Finally, differences between adiabatic and diabatic hybridization are explored. In essence, the exploratory model can be used to elucidate clearly, without distracting detail, principles of the thermodynamics underlying the process of magma hybridization. These principles are of general applicability and carry over to more compositionally complicated systems.

Toy Model Description

The phase diagram isobaric TX section of the exploratory system is depicted in Figure 2. Table 2 identifies all parameters used in the toy model. The toy system is a binary component eutectic phase diagram similar to the system $CaMgSi_2O_6$-$CaAl_2Si_2O_8$, with no crystalline solution. There are three possible phases in this system: crystals of phase α, crystals of phase β, and a liquid phase. The two components of this system are A and B with α phase pure component A and phase β pure component B. For ease of explanation, and without loss of generality, liquidii are linearized to make the analytical treatment transparent. However, curved liquidii can easily be treated. A few calculations done with curved liquidii, while giving slightly different quantitative solutions, show no large differences. Although thermodynamic parameters relevant to the system $CaMgSi_2O_6$-$CaAl_2Si_2O_8$ have been used, the point of the exploratory model is to study the principles of hybridization and not to model any particular system. Indeed, the parameters required to define the phase topology and thermodynamics can be changed in order to study their effects explicitly.

There are eight thermodynamic parameters needed to define (isobarically) the topology of the toy system. These include the eutectic composition, X_e, and temperature,

627 T_e, congruent melting temperature of pure α and β crystals (T_m^{α} and T_m^{β}) and the specific
628 (per unit mass) fusion enthalpies of α and β ($\Delta h^{\alpha}, \Delta h^{\beta}$). The remaining two parameters
629 are isobaric specific heats, one for the solids (i.e., α and β crystals), C_S and one for the
630 liquid (i.e., melt), C_L. These isobaric specific heats are constant, independent of
631 temperature and composition. This approximation alters quantitative results only slightly
632 and does not substantially affect the conclusions. In fact, at igneous temperatures, the
633 isobaric specific heats of liquids and crystals vary little with temperature and composition,
634 especially when the ranges of X and T are small. In the toy model, heats of mixing
635 associated with non-ideality are neglected. Although mixing enthalpies are generally not
636 identically zero, they are relatively small compared to fusion enthalpies and, when
637 translated into temperature differences, are of order 10-40 K. For example, in the system
638 $CaMgSi_2O_6$-$CaAl_2Si_2O_8$ the maximum excess enthalpy associated with mixing is ~60
639 kJ/kg (Sugawara and Akaogi, 2003). In comparison, the fusion enthalpies of diopside and
640 anorthite are 636 kJ/kg and 478 kJ/kg, respectively, ~ 10 times larger. The maximum
641 excess enthalpy (heat of mixing) couched in terms of a temperature difference is ~ 30 K.
642 Because the exploratory model is not meant to be representative of any natural system but
643 rather a tool to study the thermochemical principles of hybridization, these limitations do
644 not impact its implications for natural systems.
645 In addition to the eight thermodynamic parameters required to define the phase
646 diagram and mixing energetics, six additional parameters are needed to initialize the
647 system and uniquely compute the state of hybrid magma (**H**) when **M** and **R** magmas
648 completely mix to attain a hybrid state with $I \to 0$ and $\Lambda \to 0$. These parameters are: the
649 initial temperatures (T_o^M, T_o^R) and bulk compositions (X_o^M, X_o^R) of **M** and **R**, the mass
650 fraction of **M** magma (f_o) in the **M**+**R** mixture, and Φ, the ratio of the specific enthalpy
651 of the initial enthalpy sum (**M**+**R**) to hybrid (**H**) enthalpy (see below). An alternative
652 parameter, the mixing ratio defined as [$\Re$=(mass of **M**)/ (mass of **R)** where
653 $\Re = f_o/(1-f_o)$] can also be used to describe the relative masses of the mixing magmas.
654 The toy model can handle both adiabatic (isenthalpic) and diabatic magma
655 hybridization. Adiabatic mixing is for recharge treated as an isenthalpic process. Because
656 isenthalpic or R-hybridization is closed (no mass exchange with environment, only

657 homogenization of **M** and **R**) and adiabatic, the bulk composition of hybrid magma (X^H)
658 and its specific enthalpy (h^H) are identical to the initial bulk composition and specific
659 enthalpy of **M**+**R** appropriately mass-weighted according to the mixing ratio. The
660 requirement of thermodynamic equilibrium enables determination of the temperature (T^H),
661 bulk composition (X^H) and phase assemblage (mass fractions, w_α^H, w_β^H and w_ℓ^H and melt
662 composition, $X^{H\ell}$) of hybridized magma. Diabatic hybridization involves simultaneous
663 recharge and crystallization. Again, the system is closed with respect to mass but the final
664 enthalpy of the hybrid magma is set equal to some fraction Φ of the **M**+**R** weighted
665 specific enthalpy according to $h^H = \Phi h_o^{M+R}$ where $0 < \Phi < 1$. By definition, $\Phi = 1$
666 corresponds to R-hybridization since no loss of heat to the environment occurs. The
667 diabatic parameter Φ is specified upon initialization of the calculation, where $1 - \Phi$ is the
668 fraction of heat (fraction of initial **M**+**R** enthalpy) that is lost to the surroundings during
669 the recharge event. This 'lost' heat triggers crystallization above and beyond what occurs
670 in isenthalpic (adiabatic) R-hybridization, and this process is therefore termed RFC-
671 hybridization. It is noted that equilibrium and fractional crystallization produce identical
672 compositional effects in binary eutectic systems. The thermodynamic potential that is
673 maximized in R-hybridization in the entropy (Tisza, 1977). Minimization of the Gibbs
674 energy is not the appropriate action in isobaric, fixed enthalpy R-hybridization. In this
675 study, the eight thermodynamic parameters that define the phase diagram independent of
676 initial conditions are fixed at single values in order to focus specifically on effects of
677 initial conditions rather than thermodynamic properties.

678 In summary, once phase diagram topology is fixed, specification of the
679 temperature, bulk composition and mixing ratio of **M** and **R** allows the temperature, bulk
680 composition and phase assemblage and melt composition of hybrid magma to be
681 computed for a given value of the diabatic parameter. For $\Phi = 1$, the solution
682 corresponds to isenthalpic R-hybridization whereas for $0 < \Phi < 1$the mixing scenario
683 corresponds to diabatic RFC-hybridization. Figure 2 schematically depicts a typical R-
684 hybridization result based upon a phase diagram topology similar to the system
685 $CaMgSi_2O_6$-$CaAl_2Si_2O_8$ at 10^{-4} GPa. In this example, α-phyric **M** magma is mixed with
686 β-phyric **R** magma to produce a hybrid magma saturated in β at the final post-mixing

687 temperature T^H. By analogy with the system $CaMgSi_2O_6$-$CaAl_2Si_2O_8$, β can be identified
688 with anorthite and α with diopside and X_B refers to the mass fraction of $CaAl_2Si_2O_8$
689 component. A complete description and thermodynamic derivation of the toy model is
690 given in Appendix A. A downloadable spreadsheet that fully implements the toy model is
691 available at http://magma.geol.ucsb.edu/index.html. Insights gained from analysis of the
692 toy model pertaining to the thermodynamics of magma hybridization are discussed in the
693 following sections.
694
695 **Results of Application of Toy Model to Petrologic Problems**
696 Below, the toy model is used to examine a range of problems associated with the
697 thermodynamics of magma hybridization. The main goal is to examine scenarios that are
698 of potential wide application to natural systems. We show that even though the model is
699 simple, the principles carry over to magma mixing in multiphase-multicomponent natural
700 systems.
701
702 **Probability Distribution of Outcomes: Monte Carlo Simulation and a**
703 **Thermodynamic Attractor**
704 Regardless of initial conditions, the phase state of hybrid magma (i.e., post mixing
705 and equilibration) corresponds to one of five possibilities: L, α+L (if $X^H < X_e$), β+L (if
706 $X^H > X_e$), L_e+α+β or α+β, where L_e is melt of eutectic composition. It is informative to
707 study the probability distribution of phase state outcomes for R-hybridization.
708 Specifically, for fixed magma thermodynamic properties and phase relations, given a
709 reasonable range of initial values ($T_o^M, T_o^R, X_o^M, X_o^R, f_o$) describing **M** and **R**, is any
710 particular phase assemblage outcome of the five possibilities more probable than any
711 other? If there is not a stochastic (random) distribution of outcomes, what is the
712 thermodynamic principle behind the outcome probability distribution? This question is
713 addressed by Monte Carlo (MC) simulation and by analysis using the thermodynamic
714 parameters and phase diagram. The conclusion is that the invariant assemblage outcome
715 of eutectic melt coexisting with crystals of α and β (L_e+α+β) occurs significantly more
716 frequently than other outcomes. Thus, we conclude that the invariant point acts as a

'thermodynamic attractor'. The thermodynamic explanation of why this occurs is given below after MC results are presented.

The Monte Carlo approach requires defining input distributions for each of the five initial conditions on **M** and **R.** The range and population distribution statistics for each variable is given in Table 3. An MC simulation is undertaken by random selection of a particular value for each of the five initial condition parameters. This single value is randomly chosen from the range defined *ab initio*. Once individual values of each required parameter are selected, a toy model calculation is performed to generate the final hybrid magma state. Statistical analysis of 5.3 million MC simulations, based on the initial condition distributions of Table 3, gives the following for the phase assemblage distribution of **H** magma: L (6.5%), α+L (11.3%), β+L (18.5%), L_e+α+β (44%) and α+β (23 %). Since X_e (= 0.42) is less than 0.5 and the initial distributions for X^M and X^R are symmetric around 0.5 by choice, one expects, simply on compositional grounds, more L+β than L+α outcomes. Indeed this is noted in the MC results (18% vs. 11%). Similarly, because highly superheated melts, those with temperature above the melting points of α and β crystals, are avoided by choice in the initial T^M and T^R distributions, one expects more sub-solidus α+β outcomes than hyper liquidus L outcomes. This expectation is also reflected in the results (23% vs. 7%). One feature of the results is not easily rationalized from the initial distributions and phase diagram topology: the relatively large fraction of hybrid states (~44 %) at the invariant point condition of $T = T_e$, with phase assemblage L_e+α+β. That is, nearly half of all outcomes (44%) are invariant point outcomes in which three phases (L_e +α+β) coexist at the final hybrid magma temperature $T^H=T_e$. We have performed MC simulations for many other initial condition ranges and for systems with different fusion enthalpies and melting points and heat capacities and this phenomenon – a disproportionate number of invariant point outcomes – is consistently found. From these observations, we conclude that the invariant point acts as a thermodynamic 'attractor'.

The thermodynamic basis of this feature can be appreciated by examination of Figure 3. This diagram of temperature *versus* enthalpy of hybrid magma, h^H pertains to an arbitrary but fixed bulk composition X^H. The possible stable phase assemblages for

this bulk composition are separated by critical values of the enthalpy. For example, h_{max} separates the L field from the L+α (or, if $X^H > X_e$, L+β) field. If $h^H > h_{max}$, then the hybrid temperature consistent with the enthalpy of the initial state exceeds the liquidus temperature of bulk composition X^H and the final state is all L of composition $X=X^H$. h_{max} is thus the maximum value of the enthalpy such that the stable assemblage include crystals of α (or β). Similarly, when hybrid magma has a specific enthalpy between h_{mid} and h_{min}, hybrid magma will be the three-phase mixture of eutectic melt, α and β crystals (L_e+α+β). It is noted that for the particular composition X^H, h_{GMIN} and h_{GMAX} are the absolute minimum and maximum (hence 'global') values for the enthalpy consistent with the initial condition extremes of Table 3 and the specific bulk composition $X=X^H$. The significance of Figure 3 is that outcome probabilities can be predicted because the probability of a given phase assemblage outcome is proportional to the enthalpy fraction associated with that particular assemblage. For example, the probability of invariant point assemblage outcome is proportional to the fraction $(h_{mid} - h_{min})/(h_{GMAX} - h_{GMIN})$. The relatively large enthalpy interval, from h_{mid} to h_{min} portrayed in Figure 3 therefore implies that a relatively large portion of outcomes will be three-phase invariant point outcomes. The enthalpy range is large because of the latent heat effect associated with crystallization of crystalline phases α and β. Hence, the basis for the invariant point attractor is enthalpic. To summarize, there is a wide range of system enthalpies consistent with an invariant point assemblage due to the heat sink associated with crystallization effects. It is therefore expected that when crystallizing, systems remain at or near these locations in T-X space when magmas are mixed and hybridized.

Invariant Point Outcomes: A Specific Example and Application to Natural Systems

As noted, a disproportionate fraction of outcomes are three-phase invariant point ones in which eutectic liquid (L_e) stably coexists with α and β crystals. A specific example is illustrated in Figure 4. **M** magma (87% melt +12% β identified by square tie-line end points at T^M = 1580 K is mixed with **R** magma (75% melt +25% α, identified by diamond tie-line endpoints) initially at T^R = 1620 K. The fraction of **M** in the mixture is f_o= 0.7, equivalent to a mixing ratio of 2.33. Hybridized **H** magma, identified by circle

tie-line endpoints, is invariant point magma with 98% melt of eutectic composition, 1.1% α, and 1 % β crystals by mass.

The thermodynamic attractor concept is relevant to more complex multicomponent-multiphase systems because the enthalpic roots of its origin apply to multiphase-multicomponent systems, not just binary eutectic systems. The essential feature is that by virtue of the large difference in enthalpy between a liquid and solid of identical bulk composition, the invariant point state is consistent with a wide range of system specific (per unit mass) enthalpy values. Although in multicomponent systems invariant points are less common than in a simple binary system, a consequence of the phase rule, multicomponent-multiphase systems do nevertheless possess locations of low thermodynamic variance in temperature-enthalpy-composition space. These low variance states serve as multicomponent thermodynamic 'attractors' *via* the enthalpic effect. Two natural systems come to mind where invariant points may control melt compositions in RFC systems. One is the prototypical mantle system involving the ternary eutectic assemblage L + olivine + clinopyroxene + plagioclase in the shallow mantle and the assemblage L + olivine + clinopyroxene + garnet relevant to the deeper upper mantle. A second is the granite ternary system of quartz +alkali feldspar +plagioclase where the ternary minimum is a pseudo-invariant point. The fact that these two systems are relevant to magma crystallization fundamental to the generation of oceanic crust and continental crust, respectively, suggests that the petrologic 'attractor' is relevant to mantle and crustal petrology.

Melt *versus* Magma Hybridization

When resident magma (**M**) and recharge magma (**R**) are crystal-liquid mixtures, hybridization outcomes can be quite different than the case when two liquids are homogenized to give a third liquid. Below, we first present the (trivial) case of homogenization of two melts to give a third homogeneous melt. This is followed by contrasting cases that describe outcomes when magmas, not melts, are mixed. These cases highlight the differences between melt mixing and magma mixing, reveal characteristics of mixed systems that have not been previously emphasized, and show the

potential that the exploratory toy model have for providing explanations for the characteristics of particular petrologic systems.

Hybridization of melts

A degenerate application of the toy model is the state of hybrid product when two melts of distinct temperature and compositions hybridize isenthalpically (R-hybridization). It can be shown from the expressions in Tables A1 and A2 that if **M** and **R** are all liquid (or just saturated at their respective liquidus temperatures), then the resulting hybrid is also a single phase melt (or just saturated). The temperature and composition of hybridized melt are:

$$X^H = f_o X_o^M + (1 - f_o) X_o^R \quad (6)$$

$$T^H = f_o T_o^M + (1 - f_o) T_o^R \quad (7)$$

That is, the bulk composition and temperature of hybrid melt corresponds to weighted linear mixing. In general, Eq. (6) is always correct; Eq. (7) is valid strictly when the heat of mixing is identically zero (ideal mixing) as assumed in the toy model. Otherwise, a small modification to account for the heat released (negative heat of mixing) or absorbed (positive heat of mixing) upon the mixing of **M** and **R** is required. In real systems, this effect is generally rather small. The results of Eqs. (6) and (7) should be contrasted with the example below that pertains to the mixing and hybridization of magmas.

Anomalous thermal effect

Intuition suggests that when magmas mix, the temperature of the hybrid product will always lie between the temperatures of the starting magmas, **M** and **R** as given by Eq (7). That is, $T^H \in [T^M, T^R]$ in the notation of the toy model. Although true when two compositionally distinct melts mix to form a hybrid melt (as shown above), this is not necessarily the case when magmas mix. An example is illustrated in Figure 5a. **R** magma (80% melt + 20% β crystals) at initial temperature T_o^R = 1750 K is mixed into **M** magma (79% melt + 21% α crystals) at T_o^M = 1612 K and hybridized. Hybrid magma is sparsely phyric (96% melt + 4 % α) but most significantly the temperature of hybrid magma T^H is 1579 K, which is 170 degrees less than T_o^R and 33 degrees less than T_o^M. This is a

surprising result until one realizes that temperature and specific enthalpy do not share a one-to-one relationship in an equilibrium mixture of crystals plus melt. It is the enthalpy that is constant during R-hybridization; temperature is the result of the isenthalpic constraint on mixing. The temperature of hybridized magma follows from an enthalpy balance that includes sensible and latent heat effects in both **M** and **R**. In the example shown in Figure 5a, the fraction of melt in **H** is greater than the corresponding melt fractions in **M** and **R,** and yet the temperature of **H** is lower because, relative to solid, silicate liquid has a higher specific enthalpy and specific heat capacity. In Figure 5b, an additional example is presented where **M** lies on its liquidus at 1636 K where it is just saturated in α and **R** is 46 % β crystals + 54 % melt at T_o^R of 1650 K. The resultant hybrid magma is crystal-free at 1598 K which, again, is less than both T_o^M and T_o^R. Additional toy model solutions (not shown) enable one to explicitly correlate magnitude of the anomalous thermal effect with the crystal content of **R** and **M**. The magnitude of the thermal effect can be up to ~100 K for reasonable choices of initial conditions. This 'anomalous' thermal effect is therefore a robust and common outcome of magma hybridization in the toy model. Petrographically, this would be reflected in crystal resorption if earlier-formed high-temperature phenocrysts were no longer stable at the lower temperature of the hybridized magma.

The possibility of mixing hot recharge **R** melt into warm resident magma **M** and ending up with hybridized magma significantly cooler than either is not widely recognized. To investigate this phenomenon further, we have used the Magma Chamber Simulator (MCS) described by Bohrson et al. (2014) to evaluate if this phenomenon continues to be quantitatively significant in multicomponent-multiphase scenarios of isenthalpic R-hybridization. In the MCS, the thermodynamic simplifications of the toy model are not invoked. Hence, one may determine if the anomalous thermal effect applies to more realistic multicomponent-multiphase systems characterized by non-ideality in the melt and crystalline solutions, temperature and pressure dependent properties and the incorporation of H_2O and oxygen buffers and other ingredients beyond the scope of the toy model. These capabilities are, of course, missing from the exploratory toy model by intent.

Details of a relevant example are given in Table 4. Resident magma **M** of crystallinity 43 % (clinopyroxene ~17%, plagioclase ~10%, spinel ~9% and olivine ~7% by mass) and basaltic melt composition (51.2 wt. % SiO_2, 7.2 wt. % MgO, 0.6 wt. % H_2O) at 1458 K is mixed with basaltic melt **R** that is more magnesian and somewhat wetter (7.7 wt. % MgO, 2.6 wt. % H_2O) also at ~1458 K. **R** magma is at its liquidus temperature and olivine is the liquidus phase. The mixing ratio is 1.11 (f_o= 0.53); thus, roughly equal amounts of **M** and **R** are mixed and hybridized. The resulting **H** magma has a crystal content of ~13 wt. % (olivine ~6%, spinel ~5 % and clinopyroxene ~2 % by mass) and a temperature of ~1425 K. That is, T^H is ~28 K *lower* than the initial temperatures of both **M** and **R** of 1458 K. Interesting effects are also noted for the composition of hybrid melt, which is more aluminous and calcic yet poorer in FeO compared to melt in **M** and **R**. All plagioclase from **M** has been resorbed, leaving no trace in **H** magma. Several additional MCS calculations were done to quantify the relationship between the initial crystal content of **M** and the magnitude of the anomalous thermal effect. The results show that there is ~ -0.8 K change in hybrid magma temperature for every percent increase in the crystal content of **M** magma. The conclusion is that the anomalous cooling effect is not an artifact of toy model simplifications: the effect is real in the hybridization limit of magma mixing and might be expected to occur in nature. The basis of the effect is found, as outlined earlier, in the enthalpy buffering capacity of crystals. Phases with high specific (per unit mass) fusion enthalpies will be more effective in producing anomalous cooling effects. This effect should be a somewhat common effect when crystal-bearing magmas are mixed and allowed to hybridize; indicators of cooling upon mixing should be sought in the rock record. In addition, resorption is a consequence of this type of mixing. Thus disequilibrium textures indicative of resorption may originate not only from an increase in magma temperature but also a decrease. The practical importance of the anomalous thermal effect with respect to geothermometry and interpretation of common disequilibrium textures in magmatic systems remains to be more fully explored.

Digestion of stoped blocks

The toy model also allows one to investigate the thermodynamics of assimilation, which can be viewed as sub-solidus or 'cold recharge'. Daly (1903) more than a century ago defined magmatic stoping as magma emplacement due to the detachment of blocks from the roof and walls and incorporation into magma with possible reaction. Stoping itself involves a number of interrelated processes, including fracturing aided by preexisting foliation, bedding or fissility and thermal expansion, partial melting, and possible explosive exfoliation when stoped blocks include hydrous phases that become unstable upon heating (e.g., Beard et al., 2005). Many examples exist where geochemical and petrological evidence of digestive assimilation is strong. In one example, Barnes et al. (2004) provide evidence that up to 20 % by mass of the western/annular zone of the 445 Myr old Sausfjellet pluton, Norway, was derived by mixing and imperfect hybridization of resident dioritic magma with digested stoped blocks of pelitic wallrock. Another example was demonstrated by Dickin and Exley (1981) for the Redhills epigranites, Isle of Skye, northwest Scotland, which formed by mixing of 10-30 % by mass of silicic melt derived from local crust with mantle-derived differentiate. Although these complex multicomponent systems cannot be described using the toy model, the principles of digestive assimilation illuminated by the toy model most likely carry over to more complex systems. Below, we summarize three R-hybridization scenarios showing the effects of composition and temperature of stoped blocks on the state of hybrid magma.

Figures 6a and 6b illustrate the effects of cold stoped block composition on the final state of **H** magma. In these examples, initial **M** magma is 87% melt and 13 % α crystals by mass. For the conditions of Figure 6a (fraction of **M** magma equal to f_o= 0.9, stoped block is well below the solidus with a mode of 86% β and 14% α), hybridized magma **H** is ~ 28 K cooler than **M** and consists of 81% melt and 19% α crystals. **H** melt is richer in component B relative to **M** melt ($X^{H\ell} = 0.26$ vs. $X^{M\ell} = 0.16$) reflecting the β-rich mode of the stoped block. It is noted that although in this example the stoped block is β-rich, the resulting hybridized magma remains undersaturated in β phase. Thus, the influence of component B is seen not in the crystal population but in the composition of the melt. In Figure 6b, all values are identical to Figure 6a except now the stoped block mode is 86% α and 14% β crystals, the modal opposite of Figure 6a. In this case, the

928 hybridized magma temperature is only 11 K cooler than T^M but, at the same time,
929 somewhat more crystal rich (26% α crystals). Note that the initial T of the stoped block
930 (T_o^R) is identical in these cases; differences in the **H** magma are attributed to the change
931 from β-rich (Figure 6a) to α-rich (Figure 6b) blocks being assimilated and digested. The
932 smaller degree of cooling for the case illustrated in Figure 6b is due to the smaller heat of
933 fusion of β crystals relative to α crystals showing directly how thermodynamic properties
934 influence hybridization and post-mixing magma temperature.
935 In Figure 7, the effect of the temperature of stoped blocks on the state of **H**
936 magma is shown. All parameters are identical to case of Figure 6b except that the pre-
937 mixing stoped block temperature is reduced by a factor of two (from 1300 K to 650 K).
938 Hybrid magma cools to 1601 K (cf. 1611 K in Figure 6b) and the mode of **H** magma is
939 37% α crystals vs. 26% α crystals in Figure 6b. This result shows that when the mixing
940 ratio is large, the temperature of the hybridized magma is a weak function of the
941 temperature of the stoped block whereas the mode of the stoped block is more sensitive
942 to that temperature.
943 **Diabatic hybridization**
944 The examples presented above have been for adiabatic or R-hybridization. An
945 alternative, diabatic hybridization (RFC-hybridization) is a compound recharge plus
946 crystallization process. This is handled in the model by introduction of the parameter Φ,
947 which is the ratio of **H** magma enthalpy to the sum of the enthalpies of **M** and **R**, the
948 mixing magmas. For $\Phi < 1$, net heat loss occurs during the mixing process so that the
949 hybrid magma state reflects the combined effects of adiabatic recharge and crystallization
950 triggered by heat extraction per unit mass equal to $(1-\Phi)\left(h_o^M + h_o^R\right)$. This extracted heat
951 might flow into country rock and heat or partially melt it; in the toy model, if partial
952 melting does take place, the resulting melt is not mixed into the magma body. An
953 example of RFC-hybridization is portrayed in Figure 8a. **M** magma that is saturated in
954 α (79% melt + 21% α) is hybridized with **R** magma saturated in β (71% melt + 29% β).
955 The diabatic parameter is set to $\Phi = 0.8$. The hybrid state in this case is subsolidus, with
956 mass fractions of α and β of 0.55 and 0.44, respectively. The heat loss in this example is
957 sufficient to induce complete crystallization in the mixed product. This example of

958 diabatic recharge produces a vastly different final state compared to the one portrayed in
959 Figure 8b, otherwise identical except that $\Phi = 1$ for which the hybrid state is almost all
960 liquid (98% L and 2% β). These differences illustrate need for applying energy as well as
961 mass constraints when citing 'magma mixing' as a contributory cause in creating
962 variations in bulk and phase compositions in volcanic or plutonic successions at the
963 outcrop scale of order 1-100 m or greater. Clearly, a relatively small change of ~20% in
964 total enthalpy of the mixed system yields vastly different outcomes despite other
965 conditions being identical.
966 Cessation of crystallization of a phase saturated in either **M** or **R**, as illustrated in
967 Figure 8b, is not an uncommon outcome in toy model diabatic or adiabatic mixing. Even
968 for a relatively phyric **M** magma mixed with **R** at mixing ratio $\Re = 2$ (recall $\Re \equiv$ mass of
969 M /mass of R), complete resorption of α crystals occurs, and thus, in **H** magma, the
970 record of such crystallization events is erased. RFC-hybridization of magmas is a
971 possible explanation of the 'pyroxene paradox' relevant to the petrogenesis of MORB
972 (Francis, 1986) that does not rely on polybaric fractionation, as significant as the latter
973 may be. The usual resolution of the paradox is fractionation of pyroxene at depth (e.g.,
974 Bence et al., 1979; Grove et al., 1992; Dantas et al., 2007). This explanation draws
975 support from observations of melt inclusions trapped in olivine phenocrysts in the
976 absence of clinopyroxene phenocrysts that retain the fossil signature of earlier high-
977 pressure clinopyroxene crystallization and removal. The toy model calculations show that
978 magma mixing via the RFC-hybridization process can also cause cessation of phase
979 precipitation under isobaric conditions. Indeed, such a mechanism was proposed to
980 account for the 'pyroxene paradox' based on mass balance and phase equilibria
981 arguments decades ago (O'Hara, 1977; Shibata, 1979; Sullivan and DeLong, 1978;
982 Rhodes et al., 1979; Walker et al., 1979). This possibility is consistent with results of the
983 toy model, specifically RFC-hybridization under isobaric conditions. This could work in
984 the following way: **M** magma undergoes an episode of fractional crystallization whereby
985 melt in **M** develops the geochemical signature (major and trace elements) of α
986 crystallization. If this fractional crystallization event is followed by R- or RFC-
987 hybridization event, melt of hybrid **H,** will retain the α crystallization signature despite
988 its lack of α phenocrysts in **H**. If fractional crystallization is not perfect, some crystals of

989 α might be retained in **M**. These would be unstable and undergo resorption during mixing
990 and hybridization.
991
992 **Implications**
993 The geologic, petrologic, and geochemical record preserved in plutonic and
994 volcanic rocks from all major petrotectonic associations is replete with evidence of
995 magma mixing across the continuum from magma mingling to magma hybridization.
996 Along with assimilation and fractional crystallization, magma mixing is one of the pillars
997 upon which magmatic evolution depends. Petrologic indicators of magma mingling are
998 typically obvious (e.g., enclaves, mingled pumice, sieve texture, partially resorbed
999 crystals), whereas those associated with nearly hybridized magma may be "cryptic" (e.g.,
1000 zoned phenocrysts) with no naked-eye heterogeneities (e.g., Dungan, 1987; Humphreys
1001 et al., 2013). A critical issue is definition and quantification of statistical measures, such
1002 as the intensity (I) and linear scale (Λ) of segregation in light of the 'scale of scrutiny'
1003 employed by the investigator. Magmas that form as the result of hybridization may go
1004 undetected. Because dynamical analysis suggests that hybridization is not uncommon the
1005 import of developing tools to identify and describe such mixed products is obvious,
1006 particularly because mantle source characteristics are often linked to those found in
1007 basaltic products. Exploratory model results presented here have implications that impact
1008 assumptions about the petrologic consequences of mixing and highlight the need to
1009 constrain open-system petrologic models with detailed textural and chemical data and
1010 modeling using energy- and mass-constrained thermodynamic models. Among the
1011 significant implications for mixed magma systems are: (1) The relatively homogeneous
1012 bulk rock composition erupted at particular volcanoes such as Arenal (e.g., Streck et al.,
1013 2005) and Etna (e.g., Corsaro and Pompilio, 2004; Armienti et al., 1984) that show clear
1014 evidence of magma mixing may be examples of the 'attractor effect'. Because the
1015 enthalpy interval associated with an invariant or pseudo-invariant point is relatively large,
1016 a system from which heat is being extracted (i.e., a cooling magma) would be expected to
1017 reside at or remain near this special thermodynamic state. Our hypothesis is that magmas
1018 from volcanoes such as Etna and Arenal (and others like them) can be of low
1019 thermodynamic variance (phase rule), and thus erupted melt compositions (and whole-

rock compositions in cases of low crystallinity magmas) do not vary significantly despite evidence for complex subvolcanic magma processes revealed by texturally and compositionally complicated crystal populations (e.g., Streck et al., 2005; Andres et al., 2008; Ginibre and Davidson, 2014). The concept of the attractor effect may also explain low compositional variance in circumstances in which assimilation and fractional crystallization play key roles. (2) A commonly cited signature of magma hybridization is a heating event, as diagnosed by textural or compositional changes in minerals (e.g., Gagnevin et al., 2007; Rivera et al., 2014) and application of geothermometry (e.g., Campbell et al., 2009; Wark et al., 2007). The thermal and compositional outcomes of such mixing events are indeed captured by both the toy model and MCS and illustrate the case in which the final mixed magma temperature is higher than one of the mixing end-members. But toy and MCS results also reveal circumstances in which a mixed magma will have a temperature that is *cooler* than the pre-mixing temperatures of both mixing end-members. Depending on the crystal contents of the two magmas, the temperature of the hybridized magma can be many tens of degrees cooler than either end-member; the magnitude of this effect depends on the crystal content of each mixing component as well as the fusion enthalpies of the crystals involved. An outcome of such a mixing event is mineral resorption (partial or total), and thus the question that obviously arises is how will the textural and compositional responses to these "cooling" mixing events compare and contrast with those where minerals preserve evidence of a "heating" event? That is, how would the "cooling" resorption events be differentiated from those that are a consequence of mixing events that lead to increased temperature for one mixing end-member? In cases where reliable geothermometers have been used, heating events are clear, but our results indicate that the assumption that resorption is linked to heating may not be always correct. The overriding implication is that to fully document open-system magmatic processes such as mixing (and/or assimilation) quantitative thermodynamic modeling tools must be employed. (3) Case examples presented here illustrate the intimate feedback that develops among melt composition, phase abundance, and temperature. The implication is that mixed magmas (melt +crystals) respond to mixing events in ways that cannot be predicted using a two-component melt mixing approach. The literature is replete with examples of mass balance reconstruction using end-

members that are inferred from compositional trajectories. To a first-order, these are useful in constraining general mixing behavior, but to gain significant new insight into the consequences of magma mixing – petrologic and volcanological (i.e., catalysts to eruption) – a rigorous thermodynamic approach is necessary. While the spectrum of possible mixing outcomes for natural systems seems unmanageable, our work illustrates that through strategic toy and MCS modeling, a taxonomy of magma mixing is possible that can elucidate "families" of mixing behavior. The goal is to map these families or modes of mixing (e.g., crystal-rich basalt + basalt melt; crystal rich andesite with rhyolite, etc.) into diagnostic compositional and petrologic indicators. Such a working taxonomy would provide essential information, which when combined with scale-appropriate petrologic and geochemical observations, would form the basis for documenting magma mixing that is worthy of 21st Century investigation.

Acknowledgements

We thank R. Wiebe, K. Putrika and C. Miller for useful comments on earlier versions of this work. Support from the National Science Foundation grants EAR-0810127 and EAR-1427737 is gratefully acknowledged.

References Cited

Anderson, A.T. (1976) Magma mixing: petrological process and volcanological tool. Journal of Volcanology and Geothermal Research, 1, pp. 3-33.

Andres, B.J., Gardner, J.E., and Housh, T.B. (2008) Repeated recharge, assimilation, and hybridization in magmas erupted from El Chichon as recorded by plagioclase and amphibole phenocrysts. Journal of Volcanology and Geothermal Research, 175, pp. 415-426.

Appleby, S.K., Graham, C.M., Gillespie, M.R., Hinton, R.W., and Oliver, G.J.H. (2008) A cryptic record of magma mixing in diorites revealed by high-precision SIMS oxygen isotope analysis of zircons. Earth and Planetary Science Letters, pp. 105–117.

Armienti, P., Barberi, F., Innocenti, F., Pompilio, M., Romano, R., and Villari, L. (1984) Compositional variation in the 1983 and other recent Etnean lavas: insights on the shallow feeding system. Bulletin Volcanologique, 47, pp. 998–1007.

Bacon, C.R. (1986) Magmatic inclusions in silicic and intermediate volcanic rocks. Journal of Geophysical Research, 91, pp. 6091-6112.

Barnes, C.G., Dumond, G., Yoshinobu, A.S., and Prestvik, T. (2004) Assimilation and crystal accumulation in a mid-crustal magma chamber; the Sausfjellet pluton, north-central Norway. Lithos, 75(3-4), 389-412.

Baxter, S., and Feely, M. (2002) Magma mixing and mingling textures in granitoids: examples from the Galway granite, Connemara, Ireland. Mineralogy and Petrology, 76, pp. 63-74.

Beard, J.S., Ragland, P.C., and Crawford, M.L. (2005) Reactive bulk assimilation: A model for crust-mantle mixing in silicic magmas, Geology, 33, pp. 681-684.

Bence, A.E., Baylis, D., Bender, J.F. and Grove, T.L. (1979) Controls on the major and minor element chemistry of mid-ocean ridge basalts and glasses. Implications of Deep Drilling Results in the North Atlantic, 2nd Ewing Symposium, pp. 331-341.

Blake, D.H., Elwell, R.W.D., Gibson, I.L., Skelhorn, R.R., and Walker, G.P.L. (1965) Some relationships resulting from the intimate association of acid and basic magmas. Quarterly Journal of the Geological Society of London, 121, pp. 31-43.

Bohrson, W.A., Spera, F.J., Ghiorso, M.S., and Creamer, J. (2014) A tool for exploring the impact of crustal contamination; the magma chamber simulator. Mineralogical Magazine, 77(5), p. 728.

Browning, P. (1984) Cryptic variation within the Cumulate Sequence of the Oman ophiolite: magma chamber depth and petrological implications, Geological Society of London, Special Publications, 13, pp. 71-82.

Bunsen, R.W. (1851) Uber die processe der vulkanischen Gesteinbildungen Islands. Annotations of Physical Chemistry, 83, pp. 197-272.

Campbell, M.E., Hanson, J.B., Minarik, W.G., and Stix, J. (2009) Thermal history of the Bandelier magmatic system; evidence for magmatic injection and recharge at 1.61 Ma as revealed by cathodoluminescence and titanium geothermometry. Journal of Geology, 117, pp. 469-485.

Carmichael, I.S.E., Turner, F.J., and Turner, J. (1974) Igneous Petrology. McGraw-Hill, New York.

Clark, S., Spera, F.J., and Yuen, D.A. (1987) Steady state double-diffusive convection in magma chambers heated from below. The Geochemical Society, Special Publication Number 1, pp. 289-304.

Clynne, M.A. (1999) A complex magma mixing origin for rocks erupted in 1915, Lassen Peak, California. Journal of Petrology, 40, pp. 105-132.

Coltice, N. and Schmalzl, J. (2006) Mixing times in the mantle of the early Earth derived from 2-D and 3-D numerical simulations of convection. Geophysical Research Letters, 33.

Coombs, M.L., Eichelberger, J.C., and Rutherford, M.J. (2000) Magma storage and mixing conditions for the 1953-1974 eruptions of Southwest Trident volcano, Katmai National Park, Alaska. Contributions to Mineral Petrology, 140, pp. 99-118.

Corsaro. R.A., and Pompilio, M. (2004) Magma dynamics in the shallow plumbing system of Mt. Etna as recorded by compositional variations in volcanics of recent summit activity (2000-2005). Journal of Volcanology and Geothermal Research, 137, pp. 55-71.

Daly, R.A. (1903) The mechanics of igneous intrusion. American Journal of Science, 15, pp. 269- 298.

Danckwerts, P.V. (1953a) The definition and measurement of some characteristics of mixtures. Applied Scientific Research, A3, pp. 279–296.

Danckwerts, P.V. (1953b) Theory of mixtures and mixing. Research, 6, pp. 355–361.

Dantas, C., Ceuleneer, G., Gregoire, M., Python, M., Freydier, R., Warren J., and Dick, H.J.B. (2007) Pyroxenites from the Southwest Indian Ridge, 9-16°E: Cumulates from incremental melt fractions produced at the top of a cold melting regime. Journal of Petrology, 48(4), 647-660.

Davaille, A. (1999a) Two-layer thermal convection in miscible viscous fluids. Journal of Fluid Mechanics, 379, pp. 223-253.

Davaille, A. (1999b) Simultaneous generation of hotspots and superswells by convection in a heterogeneous planetary mantle. Nature, 402, pp. 756-760.

DePaolo, D.J. (1985) Isotopic studies of processes in mafic magma chambers: I. The Kigapait Intrusion, Labrador. Journal of Petrology, 26(4), pp. 925-951.

Dickin, A.P., and Exley, R.A. (1981) Isotopic and geochemical evidence for magma mixing in the petrogeneis of the coire uaigneich granophyre, Isle of Skye, N.W. Scotland. Contributions to Mineralogy and Petrology, 76(1), 98-108.

Didier, J., and Barbarin, B. (1991) Enclaves and granite petrology. Developments in Petrology, 13.

Dungan, M.A. (1987) Open system magmatic evolution of the Taos Plateau Volcanic Field, norhtern New Mexico: II the genesis of cryptic hybrids. Journal of Petrology, 28(5), pp. 955-977.

Dunham, A.C. and Wadsworth, W.J. (1978) Cryptic variation in the Rhum layered intrusion. Mineralogical Magazine, 42, pp. 347-356.

Dyson, F.J. (2000) Gravity is cool; or, why our universe is hospitable to life. Origins of Life and Evolution of the Biosphere, 30(2-4), 115.

Eales, H.V. (2002) Caveats in defining the magmas parental to the mafic rocks of the Bushveld Complex, and the manner of their emplacement; review and commentary. Mineralogical Magazine, 66(6), pp. 815-832.

Eichelberger, J.C. (1980) Vesiculation of mafic magma during replenishment of silicic magma reservoirs. Nature, 288, pp. 446-450.

Eichelberger, J.C., Chertkoff, D.G., Dreher, S.T., and Nye, C.J. (2013) Magmas in collision: rethinking chemical zonation in silicic magmas. Geology, 28(7), pp. 603-606.

Farnetani, C.Z., and Samuel, H. (2003) Lagrangian structures and stirring in the Earth's mantle. Earth and Planetary Science Letters, 206, pp. 335-348.

Francis, D. (1986) The pyroxene paradox in MORB glasses – a signature of picritic parental magmas? Letters to Nature, 319, pp. 586-589.

Furman, T., and Spera, F.J. (1985) Commingling of acid and basic magma and implications for the origin of I-type xenoliths, I Field and petrochemical relations of an unusual dike complex at Eagle Lake, Sequoia National Park, Sierra Nevada, California, USA. Journal of Volcanology and Geothermal Research, 24, pp. 151-178.

Gagnevin, D., Waight, T.E., Daly, S.T., Poli, G., and Conticelli, S. (2007) Insights into magmatic evolution and recharge history in Capraia Volcano (Italy) from chemical and isotopic zoning in plagioclase phenocrysts. Journal of Volcanology and Geothermal Research, 168, pp. 28-54.

Gibson, D., Lux, D.R., and Choate, M.A. (2003) Petrography of a "cryptic" mixed magma system – the Mount Waldo granite, coastal Maine. Atlantic Geology, 39(2).

Ginibre, C., and Davidson, J.P. (2014) Sr isotope zoning in plagioclase from Parinacota Volcano (northern Chile); quantifying magma mixing and crustal contamination, Journal of Petrology 55, pp. 1203-1238

Gonnermann, H.M., Manga, M., and Jellinek, A.M. (2002) Dynamics and longevity of an initially stratified mantle. Geophysical Research Letters, 29(10).

Grove, T.L., and Bartels, K.S. (1992) The relation between diogenite cumulates and eucrite magmas. Proceedings of the Lunar and Planetary Science Conference, 22, pp. 437-445.

Gurnis, M, and Davies, G.F. (1986) The effect of depth-dependent viscosity on convective mixing in the mantle and the possible survival of primitive mantle. Geophysical Research Letters, 13, pp. 541-544.

1199 Haller, G. (2001) Distinguished material surfaces and coherent structures in three-
1200 dimensional fluid flows. Physica D, 149, pp. 248-277.

1201 Hibbard, M.J. (1981) The magma mixing origin of mantled feldspars. Contributions to
1202 Mineralogy and Petrology, 76, pp. 158-170.

1203 Hibbard, M.J. (1991) Textural anatomy of twelve magma-mixed granitoid systems. In
1204 Enclaves and Granite Petrology, Developments in Petrology 13, J. Didier and B. Barbarin,
1205 Ed., pp. 431-443. Elsevier, Amsterdam.

1206 Humphreys, M.C.S., Edmonds, M., Plail, M., Barclay, J., Parkes, D., and Christopher, T.
1207 (2013) A new method to quantify the real supply of mafic components to a hybrid
1208 andesite. Contributions to Mineral Petrology, 165, pp. 191-215.

1209 Huppert, H.E., Sparks, R.S.J., and Turner, J.S. (1982) Effects of volatiles on mixing in
1210 calc-alkaline magma systems. Nature, 297, pp. 554-557.

1211 Irvine, T.N. (1970) Heat transfer during solidification of layered intrusions; I, sheets and
1212 sills. Canadian Journal of Earth Sciences, 7(4), pp. 1031-1061.

1213 Jellinek, A.M., and Kerr, R.C. (1999) Mixing and compositional stratification produced
1214 by natural convection; 2 applications to the differentiation of basaltic and silicic magma
1215 chambers and komatiite lava flows. Journal of Geophysical Research, 104, pp. 7203-7218.

1216 Kamber, B.S. and Collerson, K.D. (2000) Zr/Nb systematics of ocean island basalts
1217 reassessed - case for binary mixing. Journal of Petrology, 41, 1007-1021.

1218 Kellogg, L.H., and Turcotte, D.L. (1990) Mixing and the distribution of heterogeneities
1219 in a chaotically convecting mantle. Journal of Geophysical Research, 95, pp. 421-432.

1220 Koh, T.Y., and Legras, B. (2002) Hyperbolic lines and the stratospheric polar vortex.
1221 Chaos, 12, pp. 382-394.

1222 Landi, P., Metrich, N., Bertagnini, A., and Rosi, M. (2004) Dynamics of magma mixing
1223 and degassing recorded in plagioclase at Stromboli (Aeolian Archipelago, Italy).
1224 Contributions to Mineralogy and Petrology, 147, pp. 213-227.
1225
1226 Langmuir, C.H. (1989) Geochemical consequences of in situ crystallization. Nature
1227 (London), 340(6230), pp. 199-205.

1228 Larson, L., Thomas, C., Eppinga, M., and Coulthard, T. (2014) Exploratory modelling:
1229 Extracting causality from complexity. Eos, 95(32), pp. 285-292.

1230 Le Bars, M. and Davaille, A. (2002) Stability of thermal convection in two superimposed
1231 miscible viscous fluids. Journal of Fluid Mechanics, 471, pp. 339-363.
1232
1233 Le Bars, M., and Davaille, A. (2004a) Large interface deformation in two-layer thermal
1234 convection of miscible viscous fluids. Journal of Fluid Mechanics, 499, pp. 77-110.

Le Bars, M. and Davaille, A. (2004b) Whole-layer convection in an hetergeneous planetary mantle. Journal of Geophysical Research, 109.

Lesher, C.E., Spera, F.J., 2015. Thermodynamic and Transport Properties of Silicate Melts and Magma. In: Sigurdsson, H., Houghton, B., Rymer, H., Stix, J., McNutt, S. (Eds.), The Encyclopedia of Volcanoes, Academic Press, pp. 113–141.

Liu, M., Muzzio, F.J., and Peskin, R.L. (1994) Quantification of mixing in aperiodic chaotic flows. Chaos, Solutions & Fractals, 4(6), pp. 869-893.

McCallum, I.S., Raedeke, L.D., and Mathez, E.A. (1980) Investigations of the Stillwater complex; part I, stratigraphy and structure of the banded zone. American Journal of Science, 280-A, Part 1, pp. 59-87.

Morse, S.A. (2008) Compositional convection trumps silicate liquid immiscibility in layered intrusions: A discussion of 'liquid immiscibility and the evolution of basaltic magma' by Veksler et al., Journal of Petrology 48, 2187-2210. Journal of Petrology, 49(12), pp. 2157-2168.

Nakamura, M. (1995) Continuous mixing of crystal mush and replenished magma in the ongoing Unzen eruption. Geology (Boulder), 23(9), pp. 807-810.

O'Hara, M.J. (1977) Geochemical evolution during fractional crystallization of a periodically refilled magma chamber. Nature (London), 266(5602), 503-507.

Oldenburg, C.M., Spera, F.J., Yuen, D.A., and Sewell, G.H. (1989) Dynamic mixing in magma bodies; theory, simulations, and implications. Journal of Geophysical Research, 94, 9215-9236.

Olson, P., Yuen, D.A., and Balsiger, D. (1984) Mixing of passive heterogeneities by mantle convection. Journal of Geophysical Research, 89, pp. 425-436.

Ottino, J.M. (1989) The kinematics of mixing: stretching, chaos and transport. Cambridge University Press, U.K.

Pabst, A. (1928) Observations on inclusions in the granitic rocks of the Sierra Nevada. University of California Publications, 17, pp. 325-386.

Poje, A.C., and Haller, G. (1999) Geometry of cross-stream mixing in a double-gyre ocean model. Journal of Physical Oceanography, 29, pp.1649-1665.

Petrelli, M., Perugini, D., and Poli, G. (2006) Time-scales of hybridisation of magmatic enclaves in regular and chaotic flow fields: petrologic and volcanologic implications. Bulletin of Volcanology, 68, pp. 285-293.

Petrelli, M., Perugini, D., and Poli, G. (2011) Transition to chaos and implications for time-scales of magma hybridization during mixing processes in magma chambers. Lithos, 125, pp. 211-220.

Rivera, M., Thouret, J.C., Samamiego, P., and Le Pennec, J.L. (2014) The 2006-2009 activity of the Ubinas Volcano (Peru); petrology of the 2006 eruptive products and insights into genesis of andesite magmas, magma recharge and plumbing system. Journal of Volcanology and Geothermal Research, 270, pp. 122-141.

Reid, J.B., Evans, O.C., and Fates, D.G. (1983) Magma mixing in granitic rocks of the central Sierra Nevada, California. Earth and Planetary Science Letters, 66, pp. 243-261.

Rhodes, J.M., Dungan, M.A., Blanchard, D.P., and Long, P.E. (1979) Magma mixing at mid-ocean ridges: Evidence from basalts drilled near 22° N on the Mid-Atlantic Ridge. Tectonophysics, 55, pp. 35-61.

Sakuyama, M. (1984) Magma mixing and magma plumbing systems in island arcs. Bulletin Volcanologique, 47, pp. 685-703.

Salisbury, M.J., Bohrson, W.A., Clynne, M., Ramos, F.C., and Hoskin, P. (2008) Origin of the 1915 Lassen Peak eruption by magma mixing: Evidence for formation of chemically distinct plagioclase populations from crystal size distribution and in situ chemical data. Journal of Petrology, 49(10), pp. 1755-1780.

Shibata, T. (1979) Pigeonite-bearing basalts dredged from the Puerto Rico trench; a microprobe study. Marine Geology, 30(3-4), pp. 285-297.

Smith, R.L. (1979) Ash-flow magmatism. Special Papers, Geological Society of America, 180, pp. 5-28.

Sparks, R.S.J., Sigurdsson, H., and Wilson, L. (1977) Magma mixing: a mechanism for triggering acid explosive eruptions. Nature, 267, pp. 315-318.

Spera, F.J. (1992) Lunar magma transport phenomena. Geochimica et Cosmochimica Acta 56, pp. 2253-2265.

Spera, F.J. (2000) Physical properties of magma. in Encyclopedia of Volcanoes, H. Sigurdsson, Ed., pp. 71. Academic Press, San Diego.

Stelten, M.E., Cooper, K.M., Vasquez, J.A., Reid, M.R., Barfod, G.H., Wimpenny, J., and Yin, Q. (2013) Magma mixing and the generation of isotopically juvenile silicic magma at Yellowstone caldera inferred from coupling $^{238}U - ^{230}Th$ ages with trace elements and Hf isotopes in zircon and Pb isotopes in sanidine. Contributions to Mineral Petrology.

Streck, M.J., Dungan, M.A., Bussy, F., and Malavassi, E. (2005) Mineral inventory of continuously erupting basaltic andesites at Arenal volcano, Cost Rica: implications for

interpreting monotonous crystal-rich mafic arc stratigraphies. Journal of Volcanology and Geothermal Research 140, pp. 133-155.

Sugawara, T. and Akaogi, M. (2003) Heats of mixing of silicate liquid in the systems diopside-anorthite-akermanite, diopside-anorthite-forsterite, and diopside-silica. American Mineralogist, 88, pp. 1020-1024.

Sullivan, J.W., and DeLong, S.E. (1978) Major element geochemistry of north arm mt. gabbros, bay of islands ophiolite complex, Newfoundland. Abstracts with Programs - Geological Society of America, 10(2), p. 87.

Tackley, P.J. (2007) Mantle Geochemical Geodynamics. in Treatise on Geophysics Volume 7: Mantle Dynamics, D. Bercovici and G. Schubert, Ed., pp. 437-505. Elsevier, Los Angeles.

Tisza, L. (1977) Generalized Thermodynamics, M.I.T. Press, pp. 384.

Tepley, F.J. III, Davidson, J.P., Tilling, R.I., and Arth, J.G. (2000) Magma Mixing. Recharge and Eruption Histories Recorded in Plagioclase from El Chichon Volcano, Mexico. Journal of Petrology, 41, pp. 1397-1411.

Todesco, M. and Spera, F.J. (1992) Stability of a chemically layered upper mantle. Physics of the Earth and Planetary Interiors, 71, pp. 85-95.

Troll, V.R., and Schmincke, H.U. (2002) Magma Mixing and Crustal Recycling Recorded in Ternary Feldspar from Compositionally Zoned Peralkaline Ignimbrite 'A', Gran Canaria, Canary Islands, Journal of Petrology, 43, pp. 243-270.

van Keken, P.E., Ballentine, C.J., and Hauri, E.H. (2003) Convective mixing in the Earth's mantle. in Treatise on Geochemistry, Carlson, R.W., Ed., pp. 471-491. Elsevier, Los Angeles.

Vantongeren, J.A., and Mathez, E.A. (2013) Incoming magma composition and style of recharge below the pyroxenite marker, eastern Bushveld complex, South Africa. Journal of Petrology, 54(8), pp. 1585-1605.

Voth, G.A., Haller, G.H., and Gollub, J.P. (2002) Experimental measurements of stretching fields in fluid mixing. Physical Review Letters, 88(25).

Walker, D., Shibata, T., and DeLong, S. (1979). Abyssal tholeiites from the Oceanographer Fracture Zone. Contributions to Mineral Petrolology, 70, pp. 111-125.

Wager, L.R., and Brown, G.M. (1968) Layered Igneous Rocks. Oliver & Boyd, London.

Wark, D.A., Hildreth, W., Spear, F.S., Cherniak, D.J., and Watson, E.B. (2007) Pre-eruption recharge of the Bishop magma system, Geology 35, pp. 235-238.

Wiebe, R.A. (1973) Relations between coexisting basaltic and granitic magmas in a composite dike. American Journal of Science, 273, pp. 130-151.

Wiebe, R.A. (1987) Rupture and inflation of a basic magma chamber by silicic liquid. Nature, 326, pp. 69-71.

Wiebe, R. A. (1996) Mafic-silicic layered intrusions; the role of basaltic injections on magmatic processes and the evolution of silicic magma chambers. Special Paper - Geological Society of America, 315, pp. 233-242.

Wiebe R.A., and Hawkins, D. (in press) Growth and Impact of a Mafic-Silicic Layered Intrusion in the Vinalhaven Intrusive Complex, Maine. Journal of Petrology.

Wilcox, R.E. (1999) The idea of magma mixing: history of a struggle for acceptance. The Journal of Geology, 107, pp. 421-432.

Figure Captions

Figure 1: Schematic representation of initial conditions and magma properties for canonical magma mixing scenario. Magmas **M** and **R** are initially layered inside an impermeable box with adiabatic sidewalls and perfectly conducting horizontal walls. **M** and **R** possess unique compositions and properties. If **R** is denser than **M** (regardless of T or C)**,** little mixing will occur except for negligible interfacial chemical diffusion. If **R** is in its initial state less dense than **M,** mixing will rapidly initiate. When temperature and compositional differences are opposing and both contribute significantly to density, complicated unsteady mixing regimes occur. See text for discussion and Table 1 for definitions.

Figure 2: Schematic portrayal of phase relations in a typical toy model realization. **M** magma (shown in red with square tie-line endpoints) and **R** magma (shown in blue with diamond tie-line endpoints), each initially in internal equilibrium, are mixed and allowed to attain equilibrium, producing hybrid magma **H** (shown in green with circle tie-line endpoints). In the example depicted, **H** magma is saturated in β and the associated temperature is less than the initial temperatures of both **M** and **R**. See text for discussion of this anomalous thermal effect. Table 2 provides definitions of all parameters.

Figure 3: Relationship between temperature and specific enthalpy for fixed composition of **H** magma. Each possible phase assemblage of **H** magma occupies a distinct region in temperature-specific enthalpy (h) coordinates. The relatively wide enthalpy range h_{mid}-h_{min} associated with the invariant point assemblage $L_e+\alpha+\beta$, where L_e is melt of eutectic composition, is the basis of the thermodynamic 'attractor' effect. The open circles labeled h_{GMIN} and h_{GMAX} are the absolute minimum and maximum specific enthalpies, respectively, of the system defined by the reasonable but arbitrary initial conditions of Table 3 and are not of special thermodynamic significance unlike h_{min}, h_{mid} and h_{max}, which do have special thermodynamic significance: they are the specific enthalpy values that uniquely separate possible phase assemblages.

Figure 4: Illustration of thermodynamic 'attractor' effect. Crystal laden **M** (87% melt + 12 % β initally at T^M = 1580 K) and **R** (75% melt + 25% α initially at T^R = 1620 K) magmas hybridize producing magma **H**. The fraction of M in the mixture is f_o= 0.7, equivalent to a mass mixing ratio of **M** to **R** magma of $\Re$ = 2.3. It is noted that T^H is less than both T^M and T^R (the act of magma hybridization produces a cooler resultant magma (H) than either end-member M or R) and H is multiply saturated ($\alpha+\beta$) with coexisting melt of eutectic composition, L_e. The enthalpy of **H** is identical to the mass weighted sum of **M** and **R** enthalpies (Φ = 1) in this example of R-hybridization.

Figure 5: Illustration of the anomalous thermal effect. Blue diamonds represent characteristics of recharge melt and solid and triangle represents its bulk composition. (a) **R** magma (80% melt + 20% β crystals) at initial temperature T_o^R = 1750 K is hybridized with **M** magma (79% melt + 21% α crystals, represented by red squares at tie-line endpoints and triangle fulcrum indicating bulk composition) at T_o^M =1612 K. The temperature of hybrid magma **H** is less than either the initial temperatures of **M** or **R**. The enthalpy of **H** is identical to the mass weighted sum of **M** and **R** enthalpies.
(b) **M** melt at its liquidus temperature (1636 K) is hybridized with crystal-laden **R** magma (46 % β crystals + 54 % melt, 1650 K). The hybrid magma **H** is in the all-liquid region of

TX space at a temperature less than either the initial temperatures of **M** or **R**. The enthalpy of **H** is identical to the mass weighted sum of **M** and **R** enthalpies.

Figure 6: Portrayal of digestion thermodynamics of subsolidus stoped blocks **R** into **M** mush, where initial **M** magma is 87% melt and 13 % α crystals by mass. The fraction of **M** magma is 0.9 in the **M**+**R** mixture. Magma (red) squares represent initial melt and solid characteristics and triangle represents bulk composition; blue diamond represents state of **R** stoped block; green circles represent **H** magma melt and solid characteristics, and green triangle represents H magma bulk composition.
(a) The stoped block is well below the solidus with a mode of 86% β and 14% α. Hybrid magma retains no record of β present in the stoped block.
(b) Portrayal of digestion thermodynamics of subsolidus stoped blocks **R** into **M** mush (L+α). Identical condition from Figure 6a except that R is modally dominated by α instead of β.

Figure 7: Portrayal of digestion thermodynamics of subsolidus stoped blocks **R** into **M** mush (L+α) illustrating the effect of stoped block temperature on H magma outcome. Identical condition from Figure 6b except that stoped block **R** is significantly cooler.

Figure 8
(a) Illustration of RFC-hybridization. The diabatic parameter is $\Phi = 0.8$ which means that **H** magma contains 80% of the sum of the enthalpy of **M** and **R**. In this case **H** magma is entirely crystalline consisting (45% β and 55% α crystals).
(b) Illustration of cessation of crystallization effect upon addition of recharge **R** magma to resident magma **M**. In this case, **M** magma saturated in α (79% L + 21% α crystals) before mixing is brought off the α liquidus. **R** magma is 71% melt + 29% β crystals. Newly formed hybrid magma is saturated in β despite a mass-mixing ratio of **M** to **R** of 2.

Tables

Table 1a: Nomenclature and variable definitions for magma mixing dynamics

Quantity	Units	Definition
ρ	kg/m^3	Density
α_T	K^{-1}	Isobaric expansivity
α_C		Chemical expansivity
T	K	Temperature
C		Mass fraction light component
$\hat{T}$		Dimensionless temperature
$\hat{C}$		Scaled composition
g	m/s^2	Gravity acceleration
$\Delta T = T_b - T_t$	K	Temperature difference (Figure 1)
$\Delta C = C_o^M - C_o^R$		Compositional difference (Figure 1)
d	m	Total layer depth
κ	m^2/s	Thermal diffusivity
υ_R	m^2/s	Kinematic viscosity of bottom layer
D	m^2/s	Chemical diffusivity
$B = \frac{\alpha_C \Delta C}{\alpha_T \Delta T}$		Buoyancy number
$Ra = \frac{\alpha_T g \Delta T d^3}{\nu_R \kappa}$		Rayleigh number
$Le = \frac{\kappa}{D}$		Lewis number
$\nu_r = \frac{\nu_M}{\nu_R}$		Ratio of kinematic viscosities
δ	m	Thickness of diffusive interface
h_c	m	Thickness of unstable layer
η	Pa s	Dynamic viscosity
V	m/s	Velocity of Rayleigh-Taylor layer
I		Intensity of segregation
Λ	m	Linear scale of segregation
τ_i	s	Timescale of i^{th} process

1457 **Table 1b: Subscripts and superscripts**

Quantity	Definition	
R	Recharge magma	
o	Initial or reference value	
b	Bottom boundary	
M	Resident magma	
H	Hybridized magma	

1458

1459 **Table 2: Nomenclature and variable definitions for exploratory model**

Quantity	Definition (units)
X	Mass fraction component B
Y	Mass fraction component A
X_e	Eutectic composition
T_e	Eutectic temperature (K)
$T_{m.p.}^{\alpha}$	Melting point phase α (K)
$T_{m.p.}^{\beta}$	Melting point phase β (K)
Δh^{α}	Specific fusion enthalpy phase α (kJ/kg)
Δh^{β}	Specific fusion enthalpy phase β (kJ/kg)
C_S	Isobaric specific heat of solid (J/kg K)
C_L	Isobaric specific heat of liquid (J/kg K)
ΔC	C_L-C_S (J/kg K)
X_o^M	Initial mass fraction of component B in **M** magma
$X_o^{M\ell}$	Initial mass fraction of component B in **M** magma liquid
X_o^R	Initial mass fraction of component B in **R** magma
$X_o^{R\ell}$	Initial mass fraction of component B in **R** magma liquid
T_o^M	Initial T of **M** magma (K)
T_o^R	Initial T of **R** magma (K)
T_ℓ^R	Liquidus T of **R** magma of bulk composition X_o^R (K)
T_ℓ^M	Liquidus T of **M** magma of bulk composition X_o^M (K)
X^H	Mass fraction of component B in hybrid magma
$X^{H\ell}$	Mass fraction of component B in **H** magma liquid
T^H	T of hybrid magma (K)
f_o	Mass fraction of **M** magma
$\Re = \frac{f_o}{1\text{-}f_o}$	Mixing ratio, mass of **M**/mass of **R**
$h_{L\alpha}^M$	Specific enthalpy **M** magma contributes to hybrid magma if **M** magma is single phase liquid of bulk composition $X_o^M < X_e$ (J/kg)
$h_{L\beta}^M$	Specific enthalpy **M** magma contributes to hybrid magma if **M** magma is single phase liquid of bulk composition $X_o^M > X_e$ (J/kg)

$h^{M}_{\alpha+L}$	Specific enthalpy **M** magma contributes to hybrid magma when **M** magma is L+α mixture of bulk composition $X^{M}_{o} < X_{e}$ (J/kg)
$h^{M}_{\beta+L}$	Specific enthalpy **M** magma contributes to hybrid magma when **M** magma is L+β mixture of bulk composition $X^{M}_{o} < X_{e}$ (J/kg)
$h^{M}_{\alpha+\beta}$	Specific enthalpy **M** magma contributes to hybrid magma when **M** magma is $\alpha+\beta$ crystal mixture (J/kg)
$h^{R}_{L\alpha}$	Specific enthalpy **R** magma contributes to hybrid magma when **R** magma is single phase liquid of bulk composition $X^{R}_{o} < X_{e}$ (J/kg)
$h^{R}_{L\beta}$	Specific enthalpy **R** magma contributes to hybrid magma when **R** magma is single phase liquid of bulk composition $X^{R}_{o} > X_{e}$ (J/kg)
$h^{R}_{\alpha+L}$	Specific enthalpy **R** magma contributes to hybrid magma when **R** magma is L+α mixture of bulk composition $X^{M}_{o} < X_{e}$ (J/kg)
$h^{R}_{\beta+L}$	Specific enthalpy **R** magma contributes to hybrid magma when **R** magma is L+β mixture of bulk composition $X^{M}_{o} > X_{e}$ (J/kg)
$h^{R}_{\alpha+\beta}$	Specific enthalpy **R** magma contributes to hybrid magma when **R** magma is $\alpha+\beta$ crystal mixture (J/kg)
h_{max}	Specific enthalpy value at boundary between L and α+L or β+L field (J/kg)
h_{mid}	Specific enthalpy value at boundary between α+L or β+L and L_e+α+β (J/kg)
h_{min}	Specific enthalpy value at boundary between L_e+α+β and α+ β field (J/kg)
h_{GMAX}	Maximum possible initial specific enthalpy for **M**+**R** in Monte Carlo realizations (J/kg)
h_{GMIN}	Minimum possible initial specific enthalpy for **M**+**R** in Monte Carlo realizations (J/kg))
Φ	Ratio of initial **M**+**R** specific enthalpy (suitably weighted) to the specific enthalpy of the hybrid magma **H:** $h^{H} = \Phi(h^{M} + h^{R})$
w^{J}_{I}	Mass fraction of I^{th} phase (α, β or ℓ) in J^{th} subsystem (**M**, **R** or **H**)

Table 3: Initial condition values for Monte Carlo simulations

Variable	Mean value	1σ	Absolute minimum value	Absolute maximum value
X_o^M	0.5	0.3	> 0	< 1
X_o^R	0.5	0.3	> 0	< 1
T_o^R	If $X_o^R < X_e$, mean value is average of $T_{m.p.}^{\alpha}$ and 0.98 T_e	150	0.98 T_e	$T_{m.p.}^{\alpha}$
T_o^R	If $X_o^R > X_e$, mean is average of $T_{m.p.}^{\beta}$ and 0.98 T_e	150	0.98 T_e	$T_{m.p.}^{\beta}$
T_o^M	If $X_o^M < Xe$, then mean is average of $T_{m.p.}^{\alpha}$ and 0.98 T_e	150	0.98 T_e	$T_{m.p.}^{\alpha}$
T_o^M	If $X_o^M > Xe$, mean is average of $T_{m.p.}^{\beta}$ and 0.98 T_e	150	0.98 T_e	$T_{m.p.}^{\beta}$
f_o	0.5	0.3	> 0	< 1

Table 4: MCS calculation of R-hybridization

	M (f_o = 0.53)		**R**	**H**	
Phases (modal %)	melt (55.7), cpx (16.9), plag (10.3), ol (7.5), spl (9.5)		melt + trace ol	melt (87.2), cpx (1.9), ol (6.0), spl (5.0)	
T (°C)	1180		1179.2	1152.5	
Compositions (wt %):	$bulk^M$	$melt^M$	$melt^R$	$bulk^H$	$melt^H$
SiO_2	45.3	51.2	52.0	48.4	51.6
TiO_2	0.9	1.3	0.6	0.8	0.8
Al_2O_3	16.4	16.7	16.5	16.3	17.1
Fe_2O_3	1.3	0.5	1.3	1.3	0.7
Cr_2O_3	2.8	0.05	0	1.5	0.07
FeO	6.6	6.7	6.8	6.7	6.0
MgO	11.9	7.2	7.7	10.0	7.0
CaO	11.6	11.5	9.8	10.7	11.8
Na_2O	2.5	3.9	2.3	2.4	2.7
K_2O	0.1	0.2	0.4	0.2	0.3
P_2O_5	0.1	0.2	0	0.05	0.06
H_2O	0.3	0.6	2.6	1.4	1.6

Abbreviations: cpx = clinopyroxene, plag = plagioclase, ol = olivine, spl = spinel

Appendix I: Derivation of the Toy Model

Thermodynamic Parameters

The toy model is based upon the thermodynamics of an isobaric two-component (A and B) phase diagram. The definition of quantities is given in Table 1 in the text. Figure 1 gives the toy model phase diagram. X is the mass fraction of component B and Y is the mass fraction of component A such that X+Y=1 in any phase. There are three possible phases in this system: crystals of α, crystals of β, or liquid (L). Melt of eutectic composition is represented by L_e for which $X=X_e$. There are five possible phase assemblages in this system: L, α+L, β+L, L_e+α+β or the crystalline assemblage α+β. The phase diagram and thermochemistry are defined by specification of X_e, T_e, the fusion enthalpies of α (Δh^{α}) and β (Δh^{β}) at their respective melting temperatures of $T^{\alpha}_{m.p.}$ and $T^{\beta}_{m.p.}$ and a single constant isobaric specific heat for crystals of either α or β (C_S) and for melt (C_L). The liquidii of the toy model are linearized in T-X space. This approximation makes little difference to any of the basic insights gained by study of the toy model regarding magma hybridization. The characteristic concave-down shape of liquidii could easily be captured using fusion entropies and taking account of the entropy, volume and enthalpy of mixing (i.e., non ideality) as in a standard liquidus curve calculation. However, the algebra becomes more cumbersome and nothing new is gained conceptually. Hence the two branches of the liquidii in T-X space are linearized such that for $X< X_e$,

$$T_{liquidus} = \left(\frac{T_e - T^{\alpha}_{m.p.}}{X_e} \right) X + T^{\alpha}_{m.p.} \qquad (A1)$$

whereas for $X > X_e$,

$$T_{liquidus} = \left(\frac{T_e - T^{\beta}_{m.p.}}{Y_e} \right) Y + T^{\beta}_{m.p.}. \qquad (A2)$$

Characterization of the initial state of M and R magmas

Once the phase diagram, magma thermochemical properties and Φ are defined, five additional parameters are required to initialize the magma hybridization. The initial state of **M** and **R** are defined by specifying their bulk compositions (X_o^M, X_o^R), temperatures (T_o^M, T_o^R) and the fraction of **M** magma in the magma mixture (f_o). Given bulk compositions and initial temperatures of **M** and **R**, phase assemblages in each can be determined from the phase diagram (lever rule) and liquidii T-X relations. Once the phase assemblage and liquid compositions (if applicable) for **M** and **R** are known, the specific enthalpy of each can be calculated and, by appropriate weighting, the specific enthalpy of the mixture computed. When magma hybridization is isenthalpic (R-hybridization), the final enthalpy of the hybrid magma is identical to the sum of the mass weighted specific enthalpies of **M** and **R**. When the process is diabatic (RFC-hybridization), then the specific enthalpy of **H** magma is Φ times the initial enthalpy of **M**+**R,** the remainder (1-Φ) being dissipated externally. The starting assemblage of **M** and **R** depend on their bulk composition and initial temperature and hence expressions for the specific enthalpy take into account phase state and proportions. The relevant expressions are collected in Table A1, which give the contributions that **M** and **R** make to the specific enthalpy of the mixture. As one example of many initial possibilities, consider initial **M** magma of bulk composition $X_o^M < X_e$ is just at its liquidus (all melt) and that **R** magma of composition $X_o^R > X_e$ lies at a temperature between the β-saturated liquidus and the eutectic. In this case, **R** is a two-phase assemblage of β + L whereas **M** is a crystal-free liquid denoted by the subscript Lα in Table A1. In this case, the initial specific enthalpy of the mixture is given by $h_o = h_{L\alpha}^M + h_{\beta+L}^R$ which from Table A1 is:

$$h_o = f_o\left[C_S T_o^M + \Delta h^\alpha + X_o^M(\Delta h^\beta - \Delta h^\alpha) + \Delta C\left(X_o^M(T_{m.p.}^\alpha - T_{m.p.}^\beta) + (T_o^M - T_{m.p.}^\alpha)\right)\right]$$
$$+(1-f_o)\left[C_S T_o^R + \left(\frac{Y_o^R}{Y_o^{R\ell}}\right)\Delta h^\beta + Y_o^R(\Delta h^\alpha - \Delta h^\beta) + \Delta C\left(Y_o^R(T_{m.p.}^\beta - T_{m.p.}^\alpha) + \left(\frac{Y_o^R}{Y_o^{R\ell}}\right)(T_o^R - T_{m.p.}^\beta)\right)\right] \quad \text{(A3)}$$

Any combination of states of **M** and **R** can be constructed using appropriate pairs from Table A1. The composition of the melt along the liquidus in eq (A3) is found from eq (A2) by setting $T_{liquidus}$ equal to T_o^R and solving for $Y_o^{R\ell}$, the composition of melt along the β-saturated liquidus. As a second example, consider a β-saturated **M** magma that receives stoped wholly crystalline blocks of **R** of assemblage **(**α+β**)** In this case, the initial specific enthalpy of the mixed magma is:

$$f_o\left[C_S T_o^M + \left(\frac{Y_o^M}{Y_o^{M\ell}}\right)\Delta h^\beta + Y_o^M(\Delta h^\alpha - \Delta h^\beta) + \Delta C\left(Y_o^M(T_{m.p.}^\beta - T_{m.p.}^\alpha) + \left(\frac{Y_o^M}{Y_o^{M\ell}}\right)(T_o^M - T_{m.p.}^\beta)\right)\right] + (1-f_o)\left[C_S T_o^R\right] \quad (A5)$$

which accounts for the β-phase saturation of **M** and the crystalline nature of **R**.

To complete initialization of the system, the bulk composition of the hybrid magma is simply found as the mass-weighted average of **M** and **R** bulk compositions according to:

$$X^H = f_o X_o^M + (1-f_o) X_o^R \quad (A4)$$

This completes characterization of the initial state when magmas **M** and **R** are mixed and hybridized (i.e., reach thermodynamic equilibrium).

Characterization of the final phase assemblage of hybrid (H) magma

The specific (per unit mass) enthalpy h of the **H** magma is given by

$$h^H = \Phi(h^M + h^R) \quad (A5)$$

The weighted contribution of **M** and **R** to the mixture are given in Table A2. The parameter Φ defines the type of hybridization. If Φ=one, the mixing is isenthalpic (adiabatic) also called R-hybridization. If $0 < \Phi < 1$, the mixing is diabatic and termed RFC-hybridization. There are five possible state assemblage outcomes when **M** and **R** hybridize. The final hybrid magma can consist of either Liquid (L), α crystals + liquid (α+L), β crystals + liquid (β+L), eutectic liquid+α crystals+β crystals (L_e+α+β), or crystals of α and β (α+β). Solid phase identities, liquid composition and temperature are found by comparing the specific enthalpy of **H** magma computed from Eq. (A5) to

enthalpy limits defined *a priori* for the five possible outcomes. These phase assemblage limits in h-T space are depicted schematically in Figure 3 of the text. Once X^H is given, the h-T diagram for that composition can be determined using the expressions given in Table A2. The five possible final state assemblages occupy distinct regions on the h-T diagram. There are three special enthalpies on this diagram denoted h_{max}, h_{mid} and h_{min}. These values separate phase assemblages. For example, when the specific enthalpy of hybrid magma h^H of bulk composition X^H exceeds h_{max}, then the final hybridized magma must lie in the L field on the phase diagram. Similarly, if $X^H > X_e$ and $h_{mid} < h^H < h_{max}$, then hybrid magma will consist of β+L or if $X^H < X_e$, and $h_{mid} < h^H < h_{max}$, the H magma assemblage is α+L. When the hybrid magma enthalpy lies in the range $h_{min} < h^H < h_{mid}$, then the assemblage is $L_e+\alpha+\beta$ and the amount of eutectic liquid is determined by enthalpy balance. In this case, the temperature is identically equal to T_e, the eutectic temperature. Finally, if $h^H < h_{min}$, the assemblage is a mixture of α and β crystals in proportions dictated by the lever rule and the temperature is less than T_e. In summary, in order to find the final state of the hybrid magma, the value of h^H is compared to the ranges given in Table A2 to discover which of the five possible assemblage outcomes is relevant.

Characterization of the temperature and phase composition(s) of hybrid (H) magma

Once the phase state or outcome is known by comparing h^H to the limits specified in Table A2 (see Figure 3), the final state of hybrid magma can be determined. The state depends first on comparison of X^H with X_e and then on the value of h^H. The conditions and final state values are given in Table A3 when $X^H < X_e$, Table A4 is valid when $X^H > X_e$ and Table A5 is valid when $X^H = X_e$ (exactly). Note that in the latter case, the α+L or β+L fields are not possible.

As a summary example, consider the possibilities when $X^H < X_e$. From the phase diagram, the state of **H** magma can be one of four states (L, L+α, $L_e+\alpha+\beta$, $\alpha+\beta$). If $h^H > h_{max}$, then **H** is a single phase melt of composition equal to the bulk composition and its temperature is given from the expression in the first row of Table A3. If instead, $h_{mid} < h^H < h_{max}$ then the **H** magma consists of liquid plus α crystals. Simultaneous solution of the two expressions in row three of Table A3 gives T^H and the composition of melt in **H**

magma ($X^H = X^{H\ell}$) in the L+α field, thereby defining the appropriate tie line. If $h_{min} < h^H < h_{mid}$, the state is defined by the invariant point assemblage of L_e+α+β. In this case, $T^H = T_e$ and $X^{H\ell} = X_e$. The mass fractions of L_e, α and β crystals are given in row 4 of Table A3. Finally, when $h^H < h_{min}$, the assemblage is wholly crystalline (α+β crystals) in proportions given in the fifth row of Table A3. Table A4 gives analogous solutions when $X^H > X_e$ and Table A5 is appropriate when $X^H = X_e$, exactly.

Table A6 collects thermodynamic parameters that approximately model the system $CaMgSi_2O_6$-$CaAl_2Si_2O_8$ at 10^5 Pa (1-bar). The toy code can be found at the following URL http://magma.geol.ucsb.edu/. Once downloaded, a user is free to change any of the thermodynamic parameters and run computations for any binary eutectic system with known parameters.

1603 **Table A1: Enthalpy contribution expressions for M and R magmas**

$h^{M}_{L\alpha}$	$f_o\left[C_S T_o^M + \Delta h^\alpha + X_o^M(\Delta h^\beta - \Delta h^\alpha) + \Delta C\left(X_o^M(T^\alpha_{m.p.} - T^\beta_{m.p.}) + (T_o^M - T^\alpha_{m.p.})\right)\right]$
$h^{M}_{L\beta}$	$f_o\left[C_S T_o^M + \Delta h^\beta + Y_o^M(\Delta h^\alpha - \Delta h^\beta) + \Delta C\left(Y_o^M(T^\beta_{m.p.} - T^\alpha_{m.p.}) + (T_o^M - T^\beta_{m.p.})\right)\right]$
$h^{M}_{\alpha+L}$	$f_o\left[C_S T_o^M + \left(\frac{X_o^M}{X_o^{M\ell}}\right)\Delta h^\alpha + X_o^M(\Delta h^\beta - \Delta h^\alpha) + \Delta C\left(X_o^M(T^\alpha_{m.p.} - T^\beta_{m.p.}) + \left(\frac{X_o^M}{X_o^{M\ell}}\right)(T_o^M - T^\alpha_{m.p.})\right)\right]$
$h^{M}_{\beta+L}$	$f_o\left[C_S T_o^M + \left(\frac{Y_o^M}{Y_o^{M\ell}}\right)\Delta h^\beta + Y_o^M(\Delta h^\alpha - \Delta h^\beta) + \Delta C\left(Y_o^M(T^\beta_{m.p.} - T^\alpha_{m.p.}) + \left(\frac{Y_o^M}{Y_o^{M\ell}}\right)(T_o^M - T^\beta_{m.p.})\right)\right]$
$h^{M}_{\alpha+\beta}$	$f_o\left[C_S T_o^M\right]$
$h^{R}_{L\alpha}$	$(1-f_o)\left[C_S T_o^R + \Delta h^\alpha + X_o^R(\Delta h^\beta - \Delta h^\alpha) + \Delta C\left(X_o^R(T^\alpha_{m.p.} - T^\beta_{m.p.}) + (T_o^R - T^\alpha_{m.p.})\right)\right]$
$h^{R}_{L\beta}$	$(1-f_o)\left[C_S T_o^R + \Delta h^\beta + Y_o^R(\Delta h^\alpha - \Delta h^\beta) + \Delta C\left(Y_o^R(T^\beta_{m.p.} - T^\alpha_{m.p.}) + (T_o^R - T^\beta_{m.p.})\right)\right]$
$h^{R}_{\alpha+L}$	$(1-f_o)\left[C_S T_o^R + \left(\frac{X_o^R}{X_o^{R\ell}}\right)\Delta h^\alpha + X_o^R(\Delta h^\beta - \Delta h^\alpha) + \Delta C\left(X_o^R(T^\alpha_{m.p.} - T^\beta_{m.p.}) + \left(\frac{X_o^R}{X_o^{R\ell}}\right)(T_o^R - T^\alpha_{m.p.})\right)\right]$
$h^{R}_{\beta+L}$	$+(1-f_o)\left[C_S T_o^R + \left(\frac{Y_o^R}{Y_o^{R\ell}}\right)\Delta h^\beta + Y_o^R(\Delta h^\alpha - \Delta h^\beta) + \Delta C\left(Y_o^R(T^\beta_{m.p.} - T^\alpha_{m.p.}) + \left(\frac{Y_o^R}{Y_o^{R\ell}}\right)(T_o^R - T^\beta_{m.p.})\right)\right]$
$h^{R}_{\alpha+\beta}$	$(1-f_o)\left[C_s\, T_o^R\right]$

1604
1605
1606
1607
1608
1609

Table A2: Specific enthalpy boundary values separating phase assemblages

Specific enthalpy	Fields Separated	Expressions for Specific enthalpy for $X^H<X_e$ and $X^H>X_e$
h_{max}	L and α+L	$C_S(T_e - T^{\alpha}_{m.p.})\left(\frac{X^H}{X_e}\right) + C_S\,T^{\alpha}_{m.p.} + \Delta h^{\alpha} + X^H(\Delta h^{\beta} - \Delta h^{\alpha}) + \Delta C\left(X^H(T^{\alpha}_{m.p.} - T^{\beta}_{m.p.}) + \frac{X^H}{X_e}(T_e - T^{\alpha}_{m.p.})\right)$
	L and β+L	$C_S(T_e - T^{\beta}_{m.p.})\left(\frac{Y^H}{Y_e}\right) + C_S\,T^{\beta}_{m.p.} + \Delta h^{\beta} + Y^H(\Delta h^{\alpha} - \Delta h^{\beta}) + \Delta C\left(Y^H(T^{\beta}_{m.p.} - T^{\alpha}_{m.p.}) + \frac{Y^H}{Y_e}(T_e - T^{\beta}_{m.p.})\right)$
h_{mid}	α+L and L_e+α+β	$C_S T_e + \left(\frac{X^H}{X_e}\right)\Delta h^{\alpha} + X^H(\Delta h^{\beta} - \Delta h^{\alpha}) + \Delta C\left(X^H(T^{\alpha}_{m.p.} - T^{\beta}_{m.p.}) + \left(\frac{X^H}{X_e}\right)(T_e - T^{\alpha}_{m.p.})\right)$
	β+L and L_e+α+β	$C_S T_e + \left(\frac{Y^H}{Y_e}\right)\Delta h^{\beta} + Y^H(\Delta h^{\alpha} - \Delta h^{\beta}) + \Delta C\left(Y^H(T^{\beta}_{m.p.} - T^{\alpha}_{m.p.}) + \left(\frac{Y^H}{Y_e}\right)(T_e - T^{\beta}_{m.p.})\right)$
h_{min}	L_e+α+β and α+β	$C_S T_e$
h_{max}	L and α+β	$C_S T_e + \Delta h^{\alpha} + X_e(\Delta h^{\beta} - \Delta h^{\alpha}) + \Delta C\left(X_e(T^{\alpha}_{m.p.} - T^{\beta}_{m.p.}) + (T_e - T^{\alpha}_{m.p.})\right)$

1611 **Table A3: Hybrid magma state for $X^H < X_e$**

Specific enthalpy range and phase assemblage	**Hybrid system state**
$h^H > h_{max}$ **L**	$T^H = \dfrac{\Phi h_o - \Delta h^\alpha - X^H(\Delta h^\beta - \Delta h^\alpha) + \Delta C\left(T^\alpha_{m.p.} - X^H(T^\alpha_{m.p.} - T^\beta_{m.p.})\right)}{C_S + \Delta C}$ $X^{H\ell} = X^H$
$h_{mid} < h^H < h_{max}$ L+α	Simultaneous solution of the following two expressions gives $X^{H\ell}$ and T^H: $C_S T^H + \left(\dfrac{X^H}{X^{H\ell}}\right)\Delta h^\alpha + X^H(\Delta h^\beta - \Delta h^\alpha) + \Delta C\left(X^H(T^\alpha_{m.p.} - T^\beta_{m.p.}) + \left(\dfrac{X^H}{X^{H\ell}}\right)(T^H - T^\alpha_{m.p.})\right) - \Phi h_o = 0$ $T^H = (T_e - T^\alpha_{m.p.})\dfrac{X^{H\ell}}{X_e} + T^\alpha_{m.p.}$ Mass fraction α crystals: $w^H_\alpha = 1 - \dfrac{X^H}{X^{H\ell}}$ Mass fraction melt: $w^H_\ell = \dfrac{X^H}{X^{H\ell}}$
$h_{min} < h^H < h_{mid}$ L_e+α+β	$T^H = T_e$ $X^{H\ell} = X_e$ mass fraction of liquid of eutectic composition: $w^H_\ell = \dfrac{\Phi h_o - C_S T_e}{\Delta h^\alpha + X_e(\Delta h^\beta - \Delta h^\alpha) + \Delta C\left(X_e(T^\alpha_{m.p.} - T^\beta_{m.p.}) + (T_e - T^\alpha_{m.p.})\right)}$ Mass fraction β phase: $w^H_\beta = X^H - w^H_\ell X_e$ Mass fraction α phase: $w^H_\alpha = 1 - w^H_\beta - w^H_\ell$

$h^H < h_{min}$ $\alpha+\beta$	$T^H = \frac{\Phi h_o}{C_S}$ $w_\alpha^H = (1 - X^H)$ $w_\beta^H = X^H$

1612

1613 **Table A4: Hybrid magma state for $X^H > X_e$**

Specific enthalpy range	**Hybrid system state**
$h^H > h_{max}$	$T^H = \dfrac{\Phi h_o - \Delta h^\beta - Y^H(\Delta h^\alpha - \Delta h^\beta) + \Delta C\left(T^\beta_{m.p.} - Y^H(T^\beta_{m.p.} - T^\alpha_{m.p.})\right)}{C_S + \Delta C}$ $Y^{H\ell} = Y^H$
$h_{mid} < h^H\ h_{max}$	Simultaneous solution of the following expressions gives melt composition $Y^{H\ell}$ and T^H: $C_S T^H + \left(\dfrac{Y^H}{Y^{H\ell}}\right)\Delta h^\beta + Y^H(\Delta h^\alpha - \Delta h^\beta) + \Delta C\left(Y^H(T^\beta_{m.p.} - T^\alpha_{m.p.}) + \left(\dfrac{Y^H}{Y^{H\ell}}\right)(T^H - T^\beta_{m.p.})\right) - \Phi h_o = 0$ $T^H = (T_e - T^\beta_{m.p.})\dfrac{Y^{H\ell}}{Y_e} + T^\beta_{m.p.}$ Mass fraction β crystals: $w^H_\beta = 1 - \dfrac{Y^H}{Y^{H\ell}}$ Mass fraction liquid: $w^H_\ell = \dfrac{Y^H}{Y^{H\ell}}$
$h_{min} < h^H < h_{mid}$	$T^H = T_e$ $Y^{H\ell} = Y_e$ mass fraction of liquid of eutectic composition: $w^H_\ell = \dfrac{\Phi h_o - C_S T_e}{\Delta h^\beta + Y_e(\Delta h^\alpha - \Delta h^\beta) + \Delta C\left(Y_e(T^\beta_{m.p.} - T^\alpha_{m.p.}) + (T_e - T^\beta_{m.p.})\right)}$ Mass fraction α phase: $w^H_\alpha = Y^H - w^H_\ell Y_e$ Mass fraction β phase: $w^H_\beta = 1 - w^H_\ell - w^H_\alpha$

$h^H < h_{min}$	$T^H = \frac{\Phi h_o}{C_S}$ $w_\alpha^H = Y^H$ $w_\beta^H = 1 - Y^H$

Table A5: Hybrid magma state for $X^H = X_e$

Specific enthalpy range	Hybrid system state
$h^H > h_{max}$	$T^H = \frac{\Phi h_o - \Delta h^\alpha - X_e(\Delta h^\beta - \Delta h^\alpha) - \Delta C\left(T_e - T^\alpha_{m.p.} + X_e(T^\alpha_{m.p.} - T^\beta_{m.p.})\right)}{C_S}$ $X^{H\ell} = X_e$
$h_{min} < h^H < h_{max}$	$T^H = T_e$ $X^{H\ell} = X_e$ Mass fraction of liquid of eutectic composition $w_\ell^H = \frac{\Phi h_o - C_S T_e}{\Delta h^\alpha + X_e(\Delta h^\beta - \Delta h^\alpha) + \Delta C\left(X_e(T^\alpha_{m.p.} - T^\beta_{m.p.}) + (T_e - T^\alpha_{m.p.})\right)}$ Mass fraction α phase: $w_\alpha^H = (1 - w_\ell^H)(1 - X_e)$ Mass fraction β phase: $w_\beta^H = (1 - w_\ell^H)X_e$
$h^H < h_{min}$	$T^H = \frac{\Phi h_o}{C_S}$ $w_\alpha^H = 1 - X_e$ $w_\beta^H = X_e$

Table A6: Thermodynamic parameters of toy model. Parameters closely follow those in system $CaMgSi_2O_6$-$CaAl_2Si_2O_8$ at 10^5 Pa.

Thermodynamic parameter	Symbol	Value	Units
Eutectic composition, mass fraction component B	X_e	0.42	
Eutectic temperature	T_e	1547	K
Melting point of α crystals	$T^{\alpha}_{m.p.}$	1665	K
Enthalpy of fusion of α crystals at $T^{\alpha}_{m.p.}$	Δh^{α}	636	kJ/kg
Melting point of β crystals	$T^{\beta}_{m.p.}$	1830	K
Enthalpy of fusion of β crystals at $T^{\beta}_{m.p.}$	Δh^{β}	478	kJ/kg
Crystal specific isobaric heat capacity	C_S	1400	J/kg K
Liquid specific isobaric heat capacity	C_L	1600	J/kg K

Fig. 1

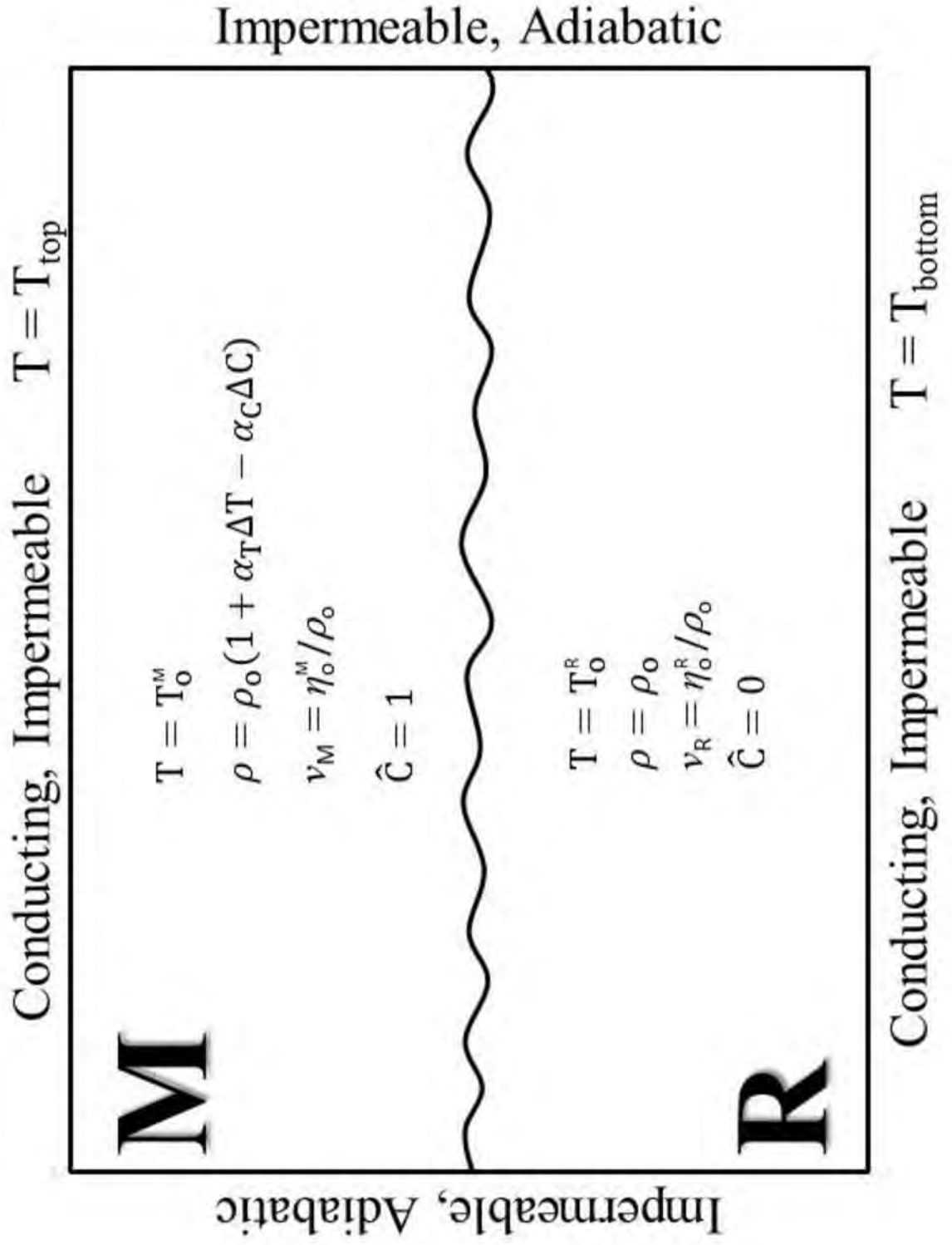
Impermeable, Adiabatic
Conducting, Impermeable T = T_top
M
T = T_o^M
ρ = ρ_o(1 + α_T ΔT − α_C ΔC)
ν_M = η_o^M/ρ_o
Ĉ = 1
R
T = T_o^R
ρ = ρ_o
ν_R = η_o^R/ρ_o
Ĉ = 0
Conducting, Impermeable T = T_bottom
Impermeable, Adiabatic

This is a preprint, the final version is subject to change, of the American Mineralogist (MSA)
Cite as Authors (Year) Title. American Mineralogist, in press.
(DOI will not work until issue is live.) DOI: http://dx.doi.org/10.2138/am-2016-5305

Fig. 2

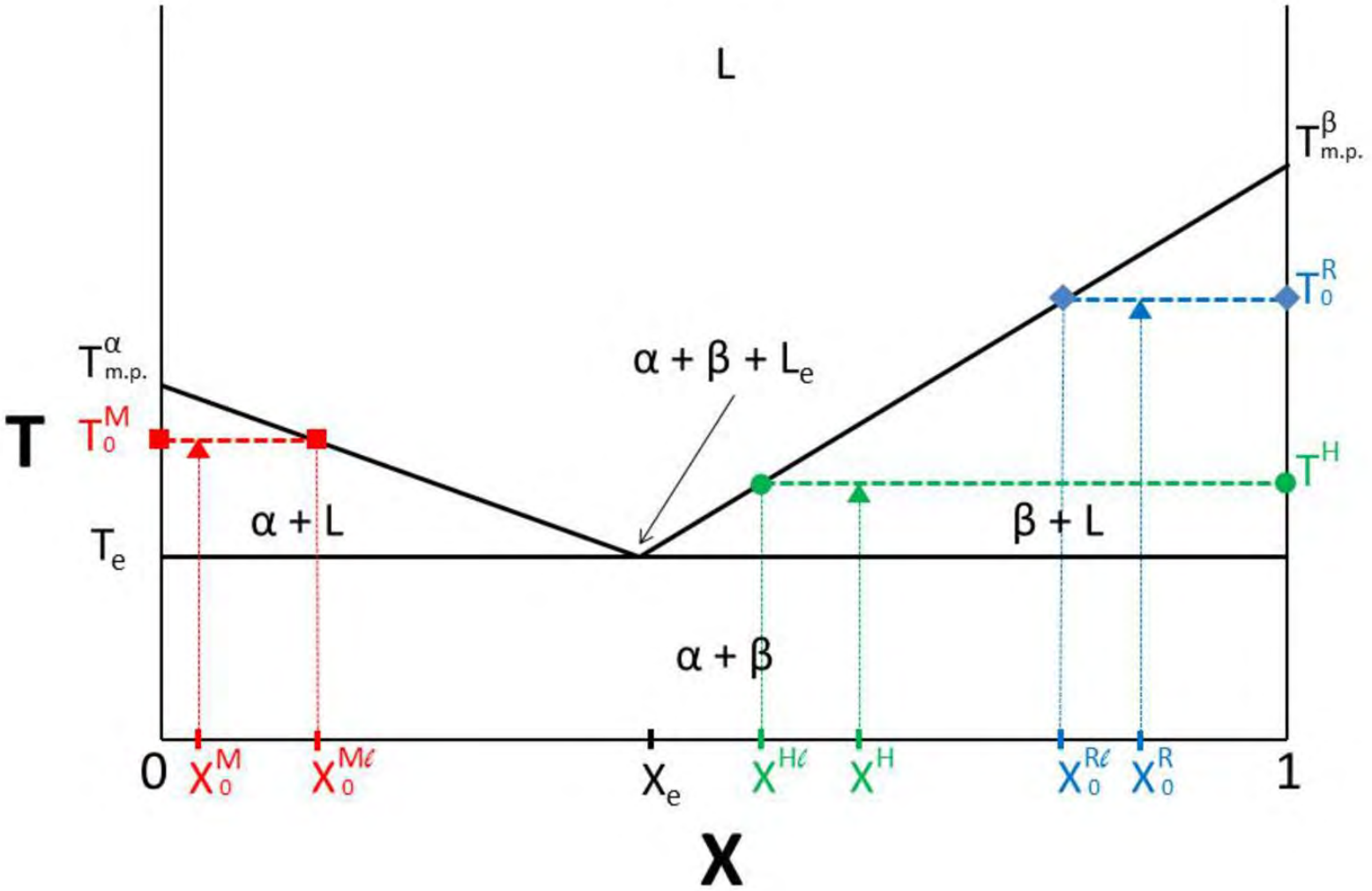

Fig. 3

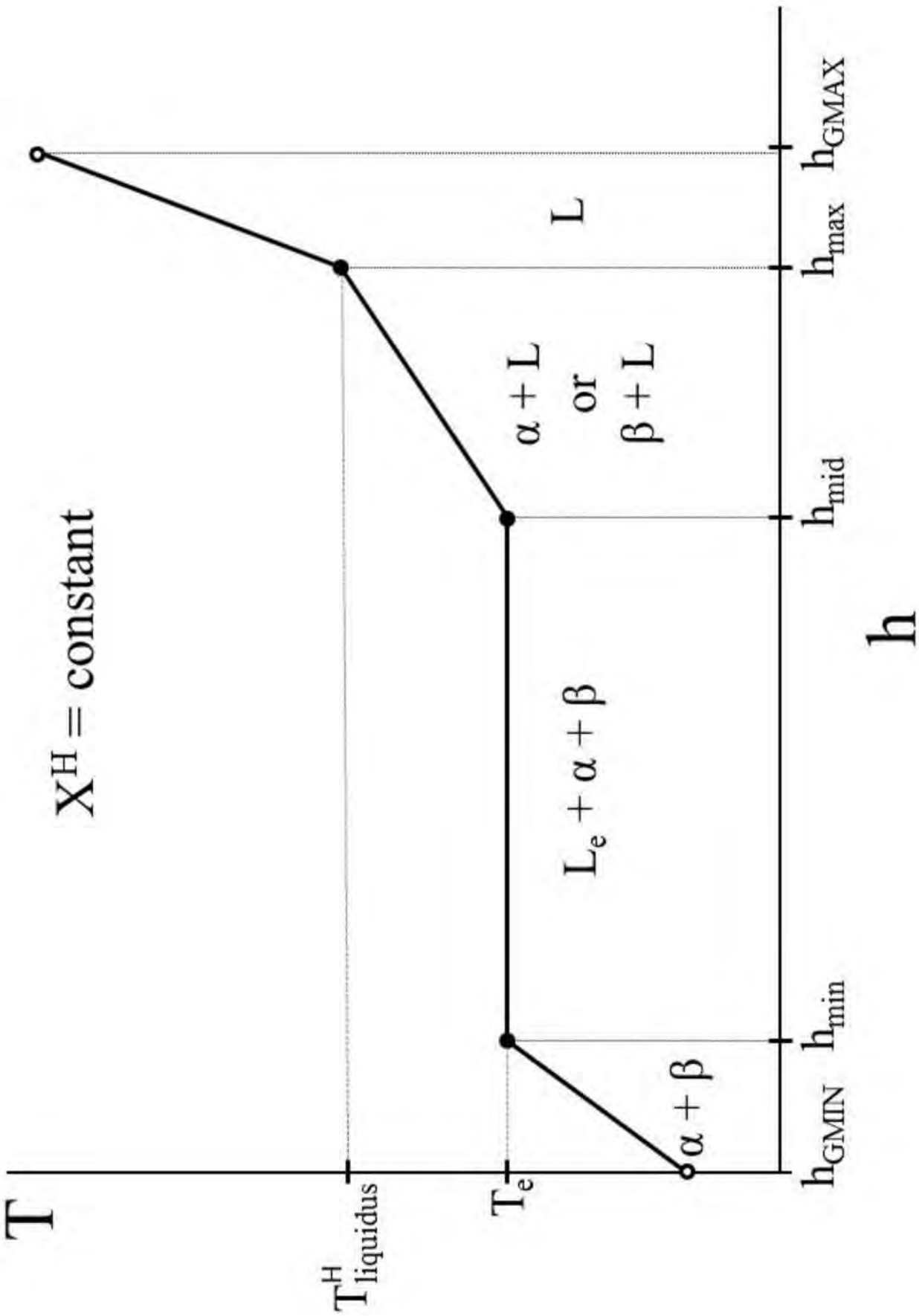
T
h
X^H = constant
$T^H_{liquidus}$
T_e
h_{GMIN}
h_{min}
h_{mid}
h_{max}
h_{GMAX}
L
α + L
or
β + L
$L_e + \alpha + \beta$
α + β

Fig. 4

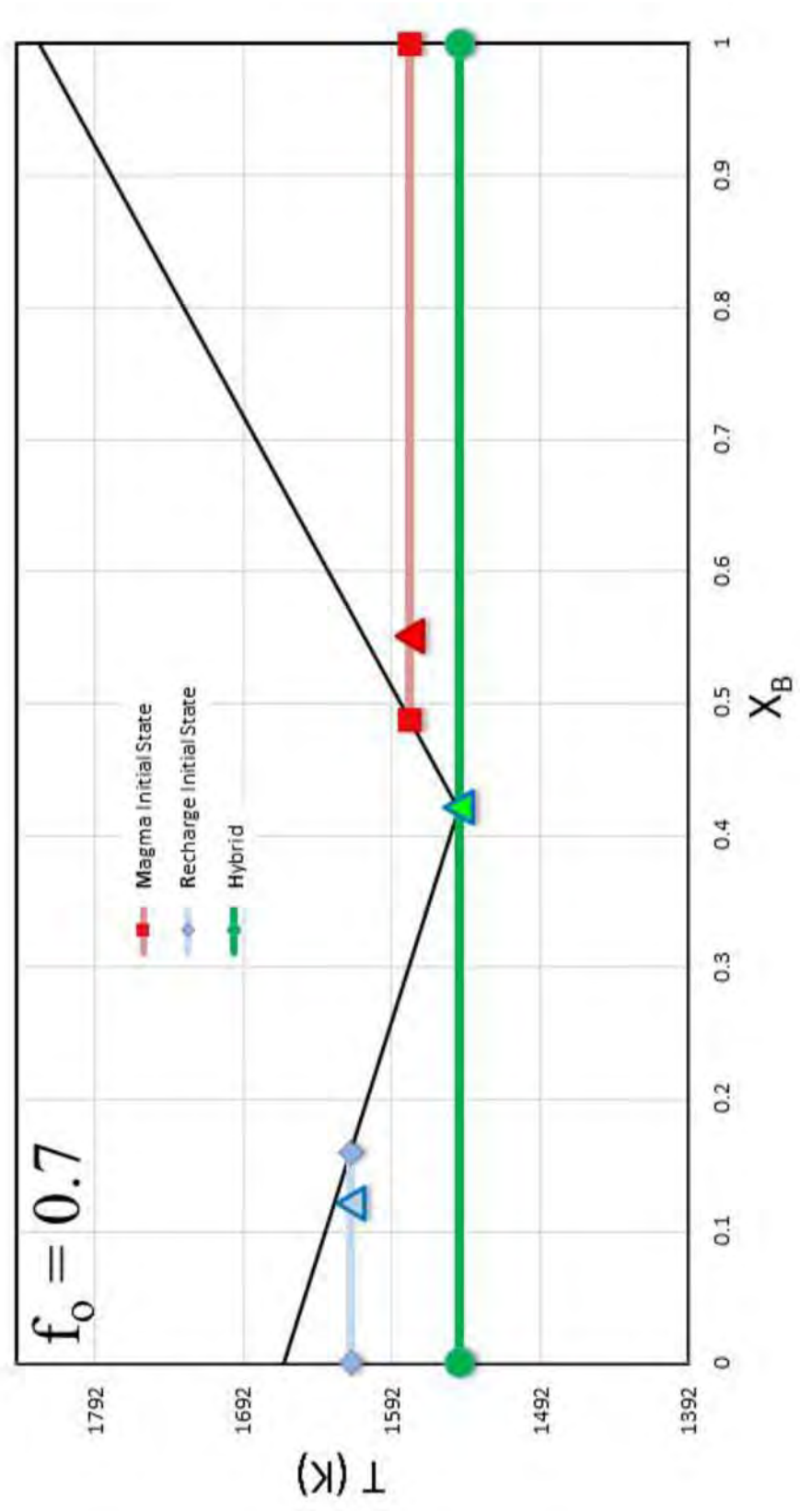
$f_O = 0.7$
Magma Initial State
Recharge Initial State
Hybrid
T (K)
1792
1692
1592
1492
1392
X_B
0
0.1
0.2
0.3
0.4
0.5
0.6
0.7
0.8
0.9
1

Fig. 5a

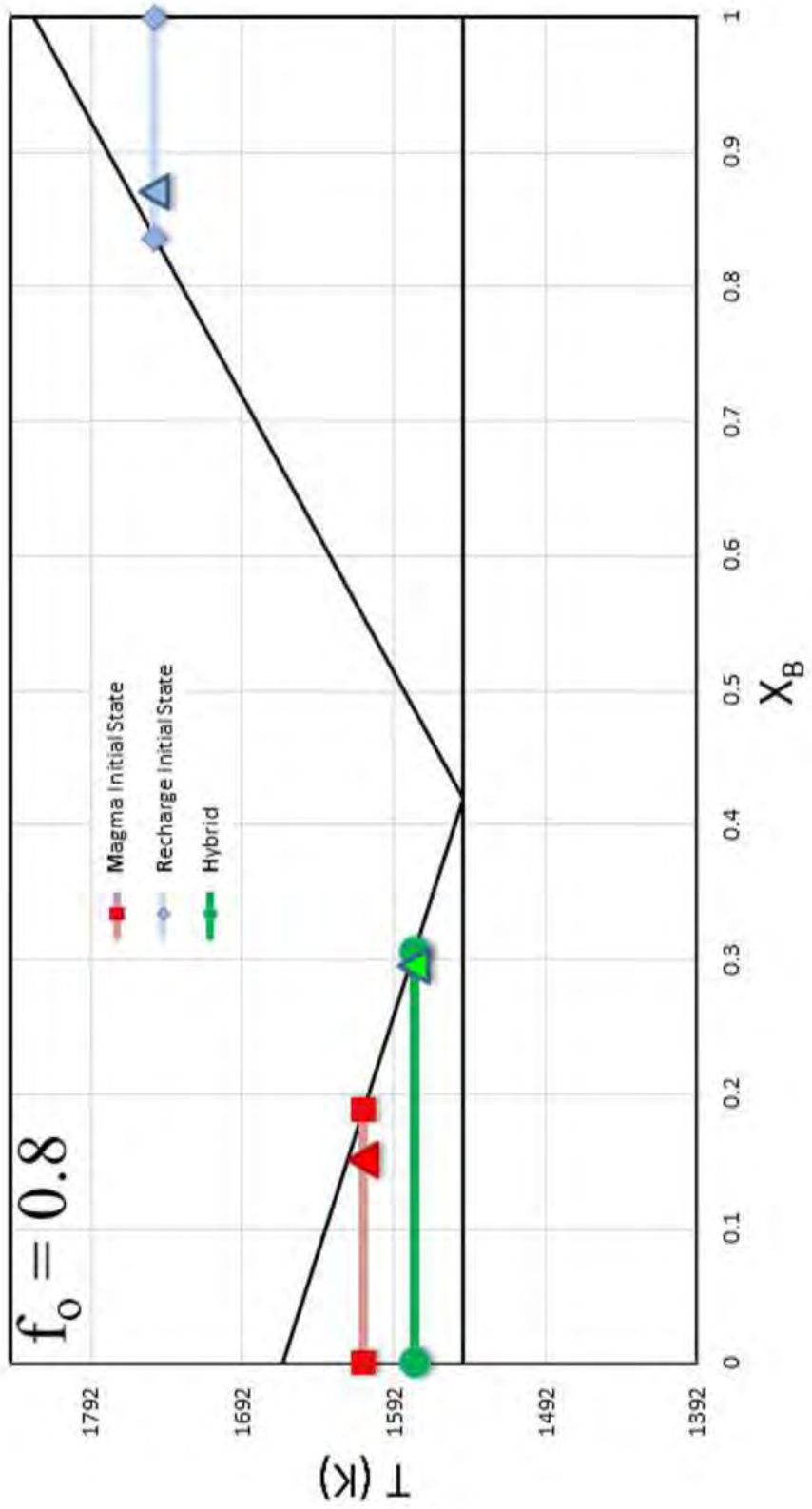
$f_o = 0.8$
Magma Initial State
Recharge Initial State
Hybrid
T (K)
1792
1692
1592
1492
1392
0
0.1
0.2
0.3
0.4
0.5
0.6
0.7
0.8
0.9
1
X_B

Fig. 5b

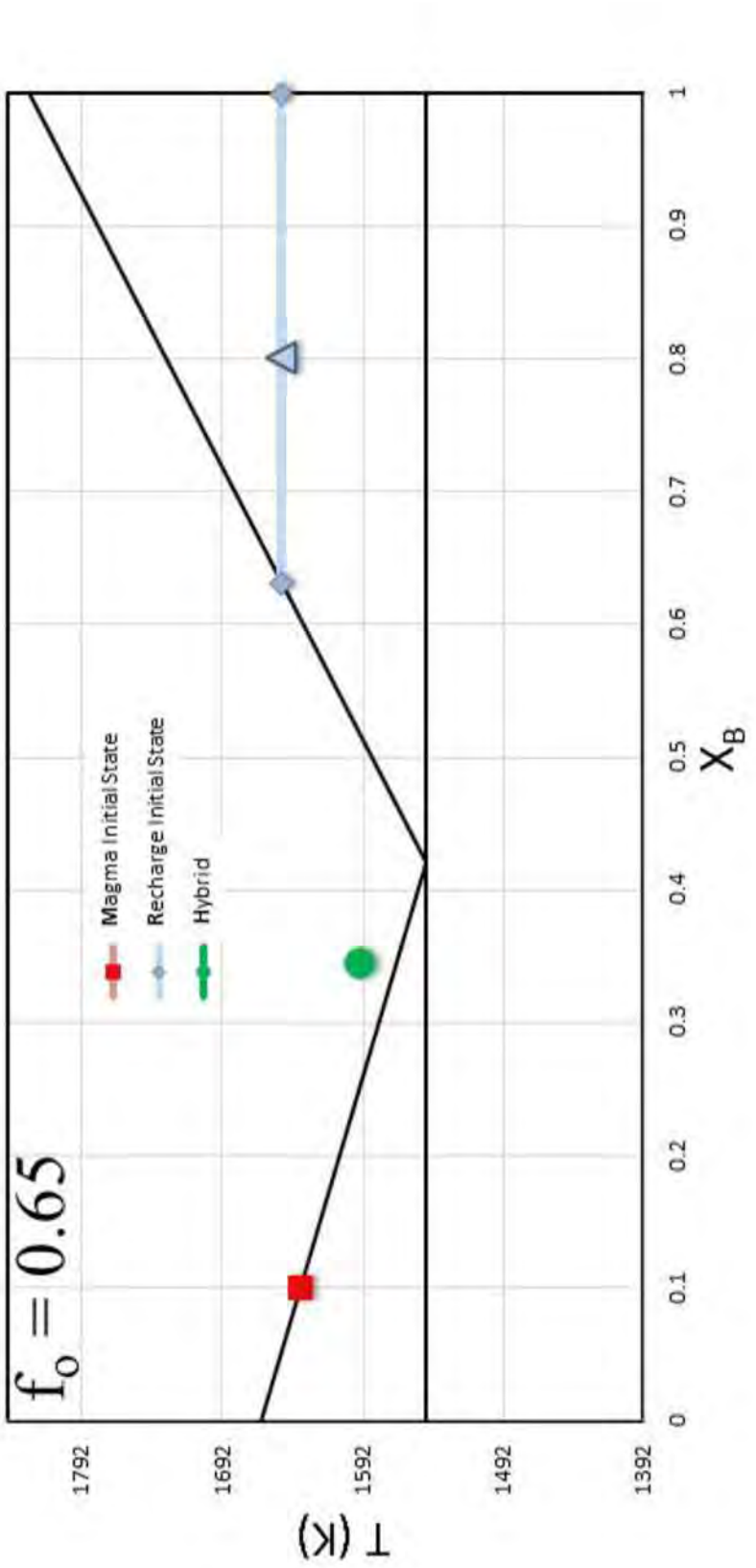
$f_o = 0.65$
Magma Initial State
Recharge Initial State
Hybrid
T (K)
1792
1692
1592
1492
1392
0
0.1
0.2
0.3
0.4
0.5
0.6
0.7
0.8
0.9
1
X_B

Fig. 6a

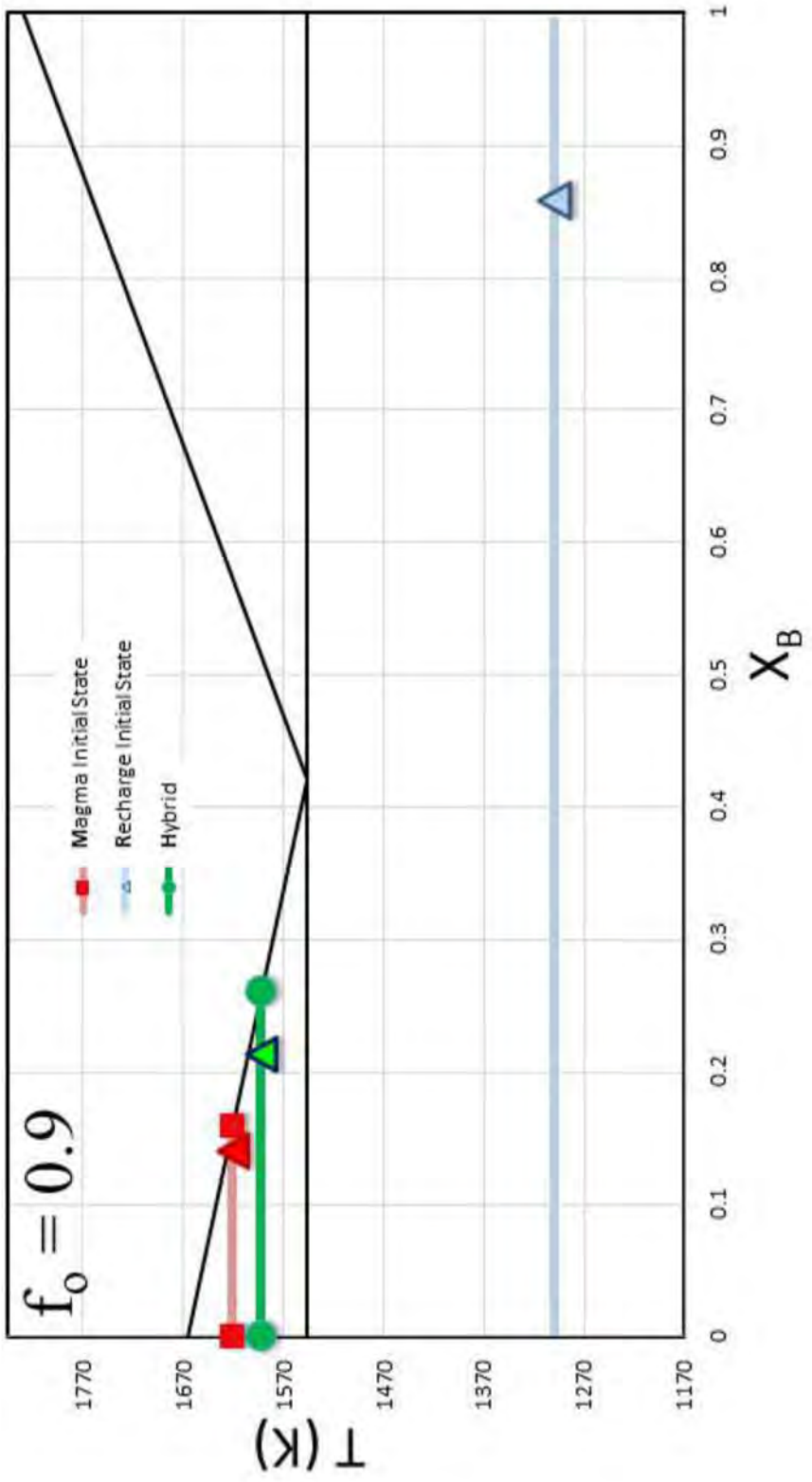
$f_o = 0.9$
Magma Initial State
Recharge Initial State
Hybrid
T (K)
1770
1670
1570
1470
1370
1270
1170
0
0.1
0.2
0.3
0.4
0.5
0.6
0.7
0.8
0.9
1
X_B

Fig. 6b

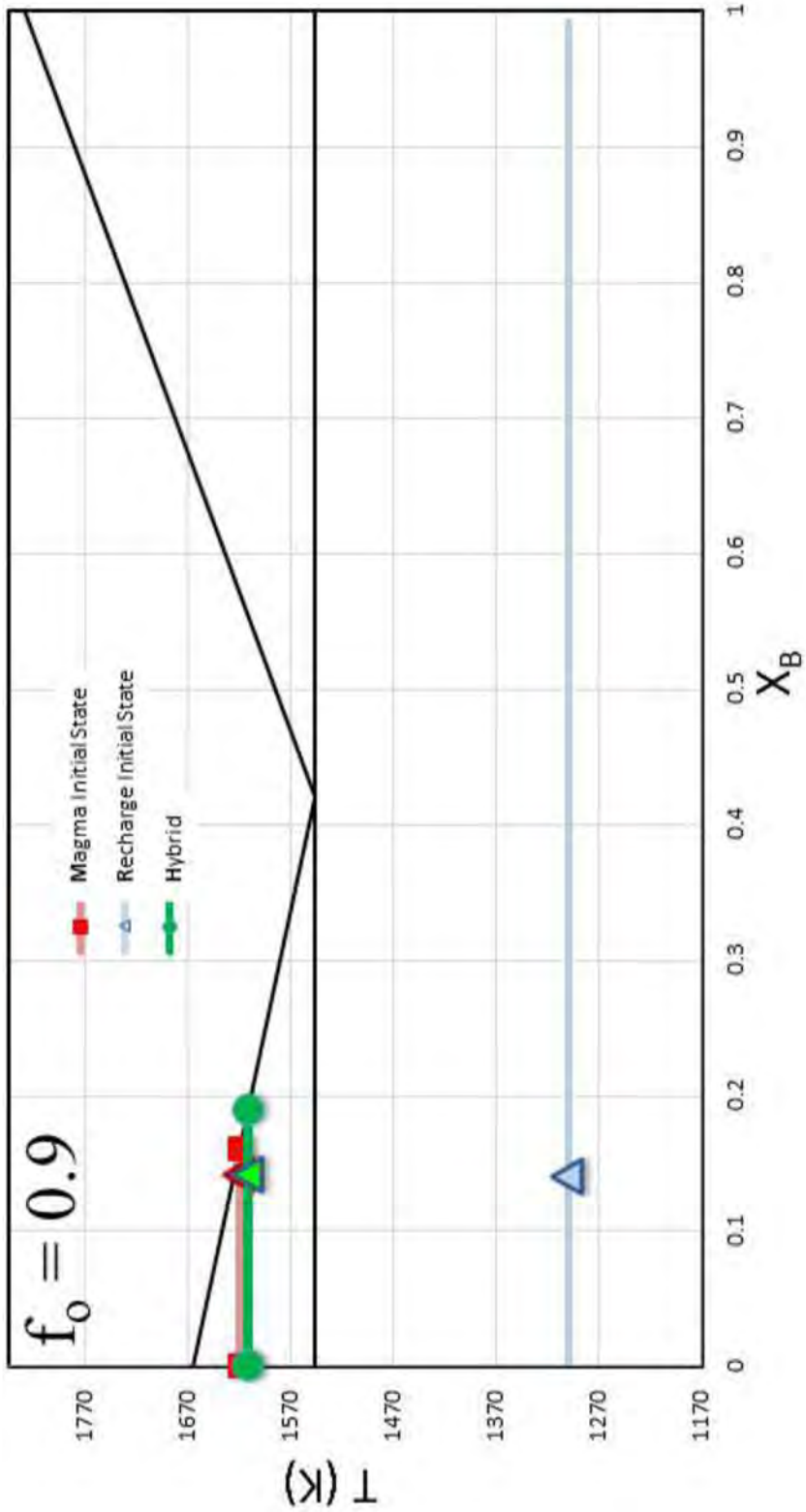
$f_o = 0.9$
Magma Initial State
Recharge Initial State
Hybrid
T (K)
1770
1670
1570
1470
1370
1270
1170
0
0.1
0.2
0.3
0.4
0.5
0.6
0.7
0.8
0.9
1
X_B

Fig. 7


T (K)
1830
1730
1630
1530
1430
1330
1230
1130
1030
930
830
730
630
0
0.1
0.2
0.3
0.4
0.5
0.6
0.7
0.8
0.9
1
X_B
$f_o = 0.9$
Magma Initial State
Recharge Initial State
Hybrid

Fig. 8a

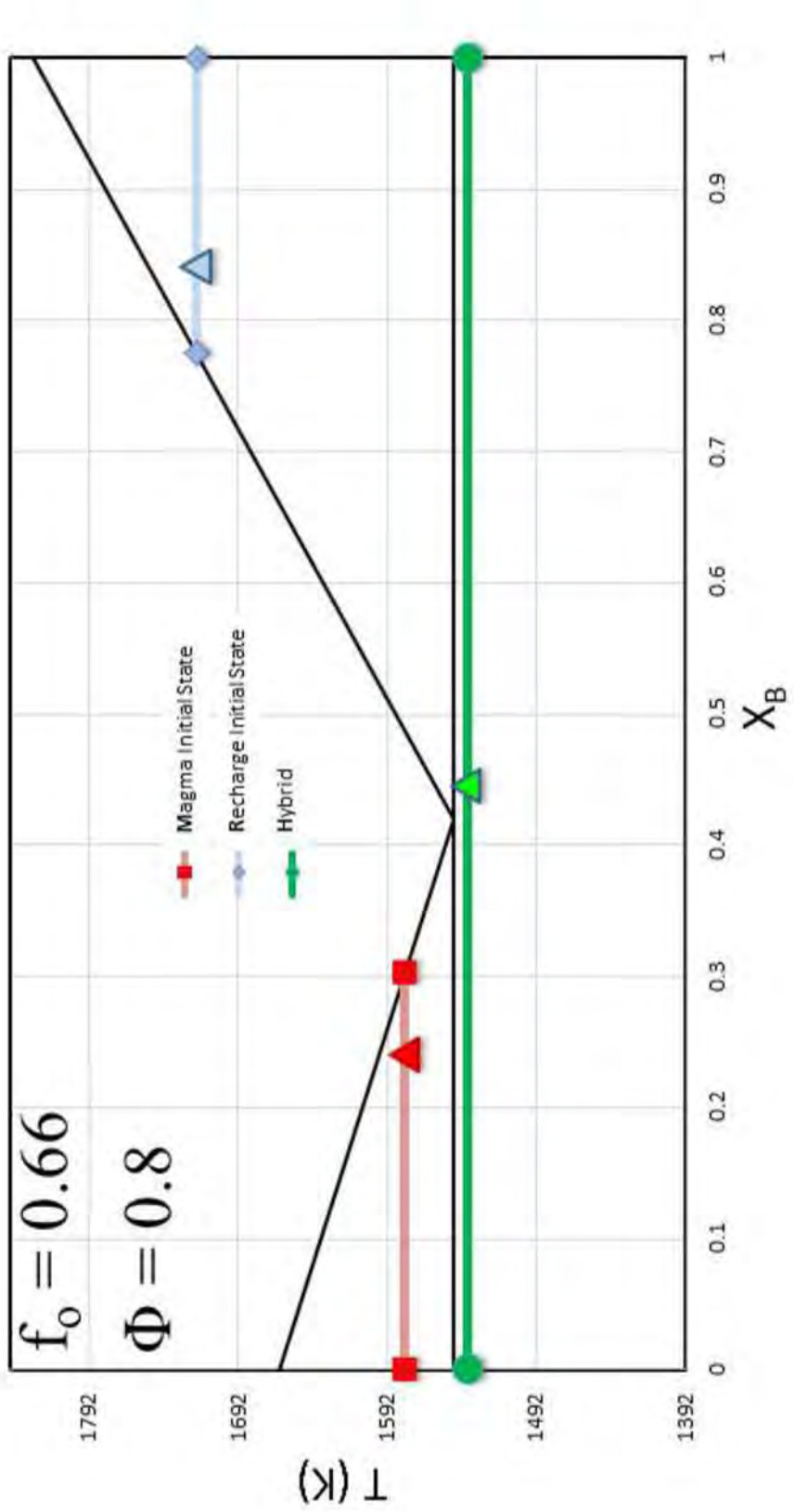
$f_o = 0.66$
$\Phi = 0.8$
Magma Initial State
Recharge Initial State
Hybrid
T (K)
1792
1692
1592
1492
1392
X_B
0
0.1
0.2
0.3
0.4
0.5
0.6
0.7
0.8
0.9
1

Fig. 8b

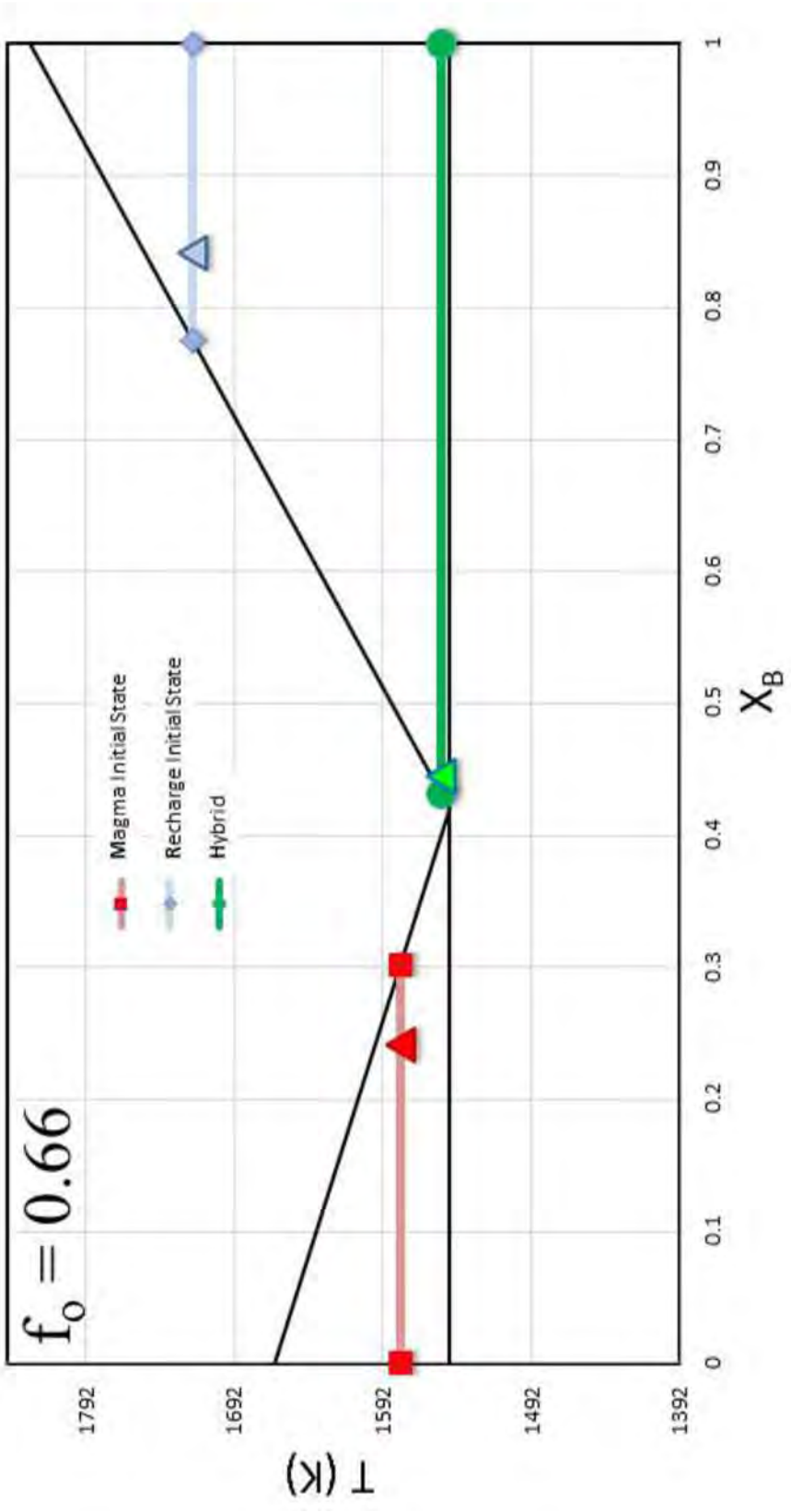
$f_O = 0.66$
Magma Initial State
Recharge Initial State
Hybrid
T (K)
1792
1692
1592
1492
1392
0
0.1
0.2
0.3
0.4
0.5
0.6
0.7
0.8
0.9
1
X_B